

TUTORIAL

## Floquet engineering with quasienergy bands of periodically driven optical lattices

To cite this article: Martin Holthaus 2016 *J. Phys. B: At. Mol. Opt. Phys.* **49** 013001

View the [article online](#) for updates and enhancements.

### Related content

- [High-frequency approximation for periodically driven quantum systems from a Floquet-space perspective](#)  
André Eckardt and Egidijus Anisimovas

- [Bloch oscillations and Zener breakdown in an optical lattice](#)  
Martin Holthaus

- [Light-induced gauge fields for ultracold atoms](#)  
N Goldman, G Juzelinas, P Öhberg et al.

### Recent citations

- [Defining a well-ordered Floquet basis by the average energy](#)  
Cristian M. Le *et al*

- [The Rabi problem with elliptical polarization](#)  
Heinz-Jürgen Schmidt

- [Krzysztof Sacha](#)



**IOP | ebooks™**

Bringing together innovative digital publishing with leading authors from the global scientific community.

Start exploring the collection—download the first chapter of every title for free.

## Tutorial

# Floquet engineering with quasienergy bands of periodically driven optical lattices

Martin Holthaus

Institut für Physik, Carl von Ossietzky Universität, D-26111 Oldenburg, Germany

E-mail: [martin.holthaus@uni-oldenburg.de](mailto:martin.holthaus@uni-oldenburg.de)

Received 22 April 2015, revised 26 August 2015

Accepted for publication 21 October 2015

Published 24 November 2015



### Abstract

A primer on the Floquet theory of periodically time-dependent quantum systems is provided, and it is shown how to apply this framework for computing the quasienergy band structure governing the dynamics of ultracold atoms in driven optical cosine lattices. Such systems are viewed here as spatially and temporally periodic structures living in an extended Hilbert space, giving rise to spatio-temporal Bloch waves whose dispersion relations can be manipulated at will by exploiting ac-Stark shifts and multiphoton resonances. The elements required for numerical calculations are introduced in a tutorial manner, and some example calculations are discussed in detail, thereby illustrating future prospects of Floquet engineering.

Keywords: optical lattices, ultracold atoms, quantum Floquet theory, multiphoton transitions, spatio-temporal Bloch waves, Floquet engineering

### 1. What this is about

The study of ultracold atoms in optical lattices by now has become a major branch of atomic physics [1–3]. In particular, increasing effort is currently being devoted to exert a controlling influence on atoms in optical lattices by subjecting them to a time-periodic external force [4–16]. Recent experiments in this fast-growing area have addressed the realization and application of artificial tunable gauge potentials [17–19], the realization of the Hofstadter Hamiltonian [20, 21], the observation of effective ferromagnetic domains [22], the realization of the topological Haldane model [23], and the creation of a roton-maxon dispersion for a Bose–Einstein condensate in a shaken optical lattice [24]. These activities indicate that ultracold atoms in periodically driven optical lattices have a high potential for simulating a wide variety of condensed-matter systems and even models of high-energy physics, thereby offering new approaches to long-standing open questions.

The theoretical tool heavily used in this emerging new field is the Floquet formalism. While this is well familiar to researchers working with atoms and molecules in strong laser fields, it does not belong to the traditional training of a cold-atoms physicist. This has led to a palpable knowledge gap:

the PhD student or postdoctoral researcher performing experiments with driven optical lattices requires an easily accessible, sharply focused introduction which should acquaint her or him with the prospects and pitfalls of the general concepts, giving advice how to perform one's own numerical simulations, and thus helping to obtain fresh ideas for specifically targeted further measurements.

The present tutorial article is intended to meet just this demand. In contrast to excellent recent review articles [25, 26] which give a fairly general overview, and explain certain approximation schemes, it is essentially a manual on how to compute, and interpret, the quasienergy band structure of a driven one-dimensional cosine lattice. Once the novice has mastered this, it will be found an easy task to adapt these methods to other situations of interest, such as more complicated lattice geometries, or different forms of driving. Besides, driven optical cosine lattices are likely to serve as the workhorses for Floquet engineering for years to come, so that the exclusive concentration on this one particular system appears to be well justified.

The material is organized as follows: in section 2 we briefly review the calculation of the energy bands of a stationary cosine lattice, in a form that will be taken up again in section 4. Before, section 3 offers a primer on the Floquet

theory of periodically time-dependent quantum systems; this could be read independently of the other parts of this paper. There we consider a deceptively simple model, the driven particle in a box. This allows us to introduce and discuss on an elementary level several facets of the Floquet picture which also govern, to a higher degree of sophistication, the physics of cold atoms in driven optical lattices. In section 4 these tools are combined, and applied to the determination of the spatio-temporal Bloch waves which form the backbones of the dynamics in time-periodically driven optical lattices. We explain the central elements required for numerical computations, and discuss the results of some selected example calculations, hoping that these may inspire the reader to explore still further parameter regimes. A short outlook given in section 5 concludes this tutorial.

A word on referencing: there exists such a wealth of papers on diverse aspects of the Floquet formalism that it is impossible to do justice to all of them. The selection of references made here naturally carries a strong personal bias, and I have to apologize to all colleagues who do not find their works properly cited. But given the availability of modern databases, a mere compilation of who did what might perhaps be found less useful than a certain pre-selection which provides a firm, definite view on the Floquet picture.

## 2. Preliminaries: band structure of a 1D cosine lattice

Let us consider a single quantum particle of mass  $M$  moving on a one-dimensional cosine lattice oriented along the  $x$ -axis, as described by the Hamiltonian

$$H(x) = -\frac{\hbar^2}{2M} \frac{d^2}{dx^2} + \frac{V_0}{2} \cos(2k_L x). \quad (1)$$

Here  $V_0$  denotes the lattice depth; in the particular case of an optical lattice  $k_L$  is the wave number of the lattice-generating laser radiation. Our first goal is to solve the stationary Schrödinger equation

$$H(x)\varphi(x) = E\varphi(x), \quad (2)$$

and thereby to determine the band structure of this lattice; this problem has been treated in great detail by Slater in the earlier days of solid-state physics [27]. To this end we introduce the dimensionless coordinate  $z = k_L x$ , so that the eigenvalue equation (2) takes the form

$$\left( -\frac{\hbar^2 k_L^2}{2M} \frac{d^2}{dz^2} + \frac{V_0}{2} \cos(2z) - E \right) \varphi(z) = 0. \quad (3)$$

Here we have sloppily but conveniently written  $\varphi(z)$  instead of the mathematically correct  $\varphi(z/k_L)/\sqrt{k_L}$ . This step allows us to identify the quantity

$$E_R = \frac{\hbar^2 k_L^2}{2M} \quad (4)$$

as the relevant energy scale of the problem; in case of an optical lattice this equals the familiar single-photon recoil

energy of the particle [1]. Dividing, we obtain

$$\left( \frac{d^2}{dz^2} + \frac{E}{E_R} - 2 \frac{V_0}{4E_R} \cos(2z) \right) \varphi(z) = 0. \quad (5)$$

This is precisely the standard form of the Mathieu equation [28],

$$\varphi''(z) + [\alpha - 2q \cos(2z)] \varphi(z) = 0, \quad (6)$$

with parameters

$$\alpha = \frac{E}{E_R}, \quad (7)$$

$$q = \frac{V_0}{4E_R}. \quad (8)$$

Therefore, the famous stability chart of the Mathieu equation, which also determines the parameters of stable ion motion in a Paul trap [29], gives essential information on the states of a particle in an optical lattice. Namely, according to the Bloch theorem [30, 31] the solutions to the eigenvalue equation (2) are Bloch waves characterized by a wave number  $k$ ,

$$\varphi_k(x) = e^{ikx} u_k(x). \quad (9)$$

In Bloch's own words, these are 'de Broglie waves which are modulated in the rhythm of the lattice structure' [30], since the functions  $u_k(x)$  inherit the periodicity of the lattice potential:

$$u_k(x) = u_k(x + \pi/k_L). \quad (10)$$

In terms of the scaled coordinate  $z$  this implies that we are looking for  $\pi$ -periodic solutions  $\varphi(z) = \varphi(z + \pi)$  to the Mathieu equation (6) when considering a band edge  $k/k_L = 0$ . The opposite edges, where  $k/k_L = \pm 1$ , then give rise to solutions which change sign after one period,  $\varphi(z) = -\varphi(z + \pi)$ , and hence are  $2\pi$ -periodic. Now it is well known that for a given value of the Mathieu parameter  $q$ , that is, for a given lattice depth, these desired periodic solutions exist only if the other parameter  $\alpha$  adopts one of the discrete so-called characteristic values  $a_r(q)$ , which produce even Mathieu functions, or  $b_r(q)$ , which belong to odd functions; while even indices  $r$  designate  $\pi$ -periodic functions, odd indices refer to  $2\pi$ -periodic ones [28]. Therefore, a plot of these characteristic values, such as depicted in figure 1, immediately allows one to read off the width of the energy bands: for  $n = 0, 1, 2, \dots$ , the (energetically) lower edge of the  $n$ th band is given by

$$E_n^{\text{lower}} = a_n(q) E_R, \quad (11)$$

while its upper edge is

$$E_n^{\text{upper}} = b_{n+1}(q) E_R; \quad (12)$$

note that the state with  $k/k_L = 0$  alternates between the lower and the upper edge from band to band.

In order to compute the full dispersion relations  $E_n(k)$  of the cosine lattice we insert the Bloch ansatz (9) into the eigenvalue equation (2), employing the momentum operator

$$p = \frac{\hbar}{i} \frac{d}{dx}, \quad (13)$$

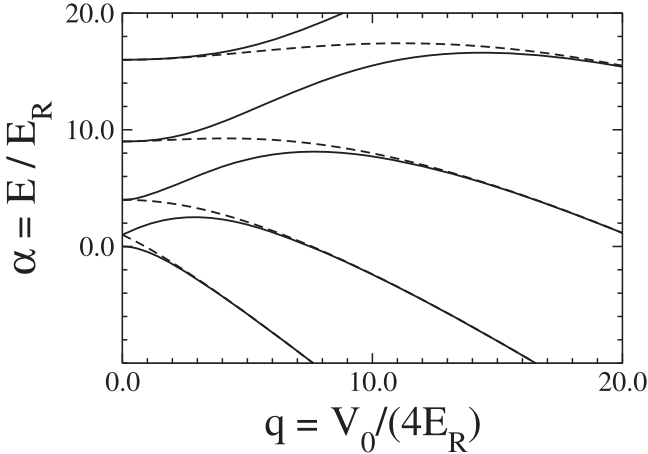


**Figure 1.** Characteristic values  $a_0, a_1, a_2, a_3, a_4$  (full lines, bottom to top) and  $b_1, b_2, b_3, b_4$  (dashed lines, bottom to top). For given scaled lattice depth  $q = V_0/(4E_R)$ , the  $n$ th energy band of a 1D optical cosine lattice ranges from  $a_n(q)$  to  $b_{n+1}(q)$ , in units of the recoil energy  $E_R$ .

thus obtaining

$$\left( \frac{p^2}{2M} + \frac{V_0}{2} \cos(2k_L x) \right) e^{ikx} u_k(x) = E(k) e^{ikx} u_k(x). \quad (14)$$

This form of the eigenvalue problem is not practical, because here the eigenfunctions consist of both the plane-wave factors  $e^{ikx}$  and the Bloch functions  $u_k(x)$ , while one has to impose the periodic boundary condition (10) on the latter only. Therefore, in the spirit of the  $k \cdot p$ -approach to band structures [32] one multiplies this equation (14) from the left by  $e^{-ikx}$  and utilizes the identity

$$\begin{aligned} e^{-ikx} p e^{ikx} &= p - ik[x, p] \\ &= p + \hbar k, \end{aligned} \quad (15)$$

arriving at

$$\left( \frac{(p + \hbar k)^2}{2M} + \frac{V_0}{2} \cos(2k_L x) \right) u_k(x) = E(k) u_k(x). \quad (16)$$

Multiplying out the squared momenta, this gives

$$\begin{aligned} \left( \frac{p^2}{2M} + \frac{\hbar k \cdot p}{M} + \frac{\hbar^2 k^2}{2M} + \frac{V_0}{2} \cos(2k_L x) \right) u_k(x) \\ = E(k) u_k(x). \end{aligned} \quad (17)$$

This modified eigenvalue equation for the Bloch functions alone is much easier to deal with than its antecessor (14), because one now can expand the eigenfunctions with respect to a suitable basis which already incorporates the periodic boundary conditions, then represent all operators in this basis, and diagonalize the resulting matrices numerically. Specifically, upon return to the dimensionless coordinate  $z = k_L x$

and division by  $E_R$  we have

$$\begin{aligned} &\left( -\frac{d^2}{dz^2} + 2 \frac{k}{k_L} \frac{1}{i} \frac{d}{dz} + \left( \frac{k}{k_L} \right)^2 + \frac{V_0}{2E_R} \cos(2z) \right) u_k(z) \\ &= \frac{E(k)}{E_R} u_k(z), \end{aligned} \quad (18)$$

requiring  $\pi$ -periodic solutions

$$u_k(z) = u_k(z + \pi). \quad (19)$$

In order to satisfy these boundary conditions we simply choose the basis  $\{\varphi_\mu(z); \mu = 0, 1, 2, 3, \dots\}$  of normalized  $\pi$ -periodic trigonometric functions, so that

$$\varphi_0(z) = \sqrt{\frac{1}{\pi}} \quad (20)$$

and

$$\varphi_\mu(z) = \begin{cases} \sqrt{\frac{2}{\pi}} \sin([\mu + 1]z); & \mu = 1, 3, 5, \dots, \\ \sqrt{\frac{2}{\pi}} \cos(\mu z); & \mu = 2, 4, 6, \dots. \end{cases} \quad (21)$$

In this basis the negative second derivative is represented by a diagonal matrix with quadratically growing entries,

$$-\frac{d^2}{dz^2} = \begin{pmatrix} 0 & & & & \\ & 4 & & & \\ & & 4 & & \\ & & & 16 & \\ & & & & 16 \\ & & & & & \dots \end{pmatrix}, \quad (22)$$

whereas the first derivative leads to a matrix with entries on the first off-diagonal only,

$$\frac{d}{dz} = \begin{pmatrix} 0 & & & & \\ & 0 & -2 & & \\ & 2 & 0 & 0 & \\ & & 0 & -4 & \\ & & & 4 & 0 \\ & & & & \dots \end{pmatrix}. \quad (23)$$

Finally, the cosine potential has nonvanishing matrix elements only on the second off-diagonal,

$$\cos(2z) = \frac{1}{2} \begin{pmatrix} 0 & 0 & \sqrt{2} & & & \\ 0 & 0 & 0 & 1 & & \\ \sqrt{2} & 0 & 0 & 0 & 1 & \\ 1 & 0 & 0 & 0 & 0 & 1 \\ 1 & 0 & 0 & 0 & 0 & \dots \\ 1 & 0 & 0 & & & \dots \end{pmatrix}. \quad (24)$$

In all these matrices (22)–(24), elements not shown are zero. Given the lattice depth  $V_0/E_R$ , one can then for any  $k/k_L$  set up the matrix corresponding to the operator on the left-hand side of equation (18), and diagonalize, making sure that the matrix size is chosen sufficiently large so that the desired eigenvalues are converged to the accuracy specified.

In figure 2 we show the dispersion relations  $E_n(k)$  for the lowest three bands  $n = 0, 1, 2$  of an optical cosine lattice with depth  $V_0/E_R = 4.0$  and  $V_0/E_R = 8.0$ , respectively; these

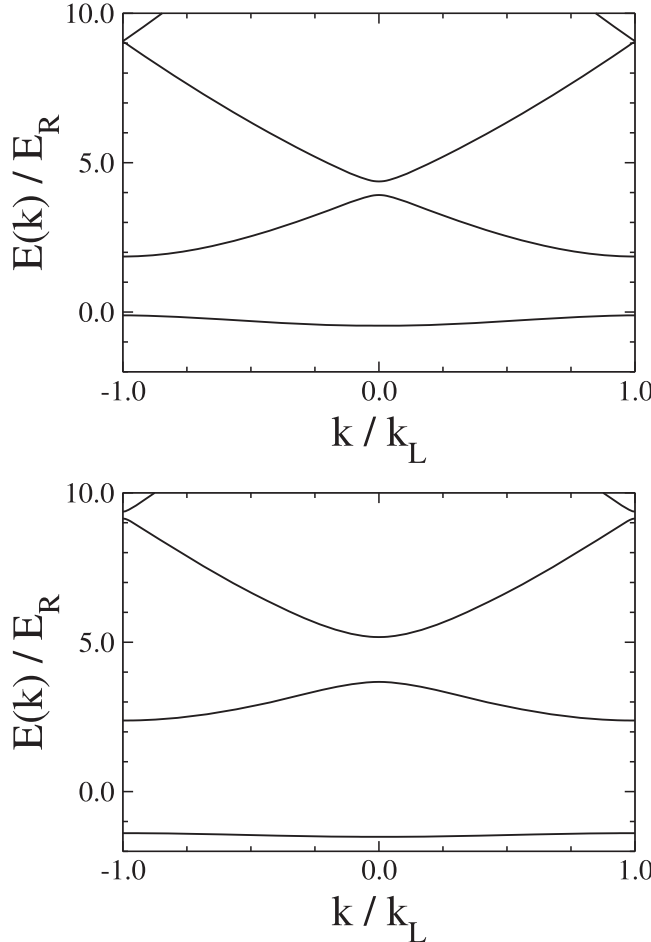


**Figure 2.** Dispersion relations  $E_n(k)$  for the lowest three bands  $n = 0, 1, 2$  of a cosine lattice with depth  $V_0/E_R = 4.0$  (upper panel) or  $V_0/E_R = 8.0$  (lower panel), restricted to the first Brillouin zone. Observe the widening of the gaps with increasing lattice depth.

two examples will be taken up again in section 4 for illustrating the engineering options offered by a time-periodic force. Since the lattice period is  $a = \pi/k_L$ , the first Brillouin zone  $-\pi/a < k \leq +\pi/a$  here ranges from  $-k_L$  to  $+k_L$  in  $k$ -space; if necessary, the dispersion relations outside this interval are obtained by periodic continuation,  $E_n(k) = E_n(k + 2k_L)$  [31].

### 3. Tools: basic elements of the Floquet picture

We now put together some elements which are required for the description of quantum systems possessing a discrete translational invariance in time rather than in space. In essence, these go back to the work of the French mathematician Achille Marie Gaston Floquet (1847–1920) on linear differential equations with periodic coefficients [33], as does Bloch's analysis of the quantum mechanics of electrons in crystal lattices [30]. But there are some peculiarities of time-periodic quantum systems which, although they are known in principle [34–42], appear to be rarely appreciated, so that this condensed summary may be found useful. Since there are no

principal differences between single-particle and many-body systems on this level, we keep this account fairly general.

#### 3.1. Mathematical foundation

Thus, we consider a quantum system defined on a Hilbert space  $\mathcal{H}$  and governed by a Hamiltonian which is periodic in time with period  $T$ ,

$$H(t) = H(t + T), \quad (25)$$

and we aim at exploring the consequences of this periodicity for the solutions to the time-dependent Schrödinger equation,

$$i\hbar \frac{d}{dt} |\psi(t)\rangle = H(t) |\psi(t)\rangle. \quad (26)$$

Here we employ the abstract bra-ket notation for quantum states, so that, for instance,  $\psi(x, t) = \langle x|\psi(t)\rangle$ . Instead of solving equation (26) for one particular initial condition we desire a characterization of *all* its solutions, so that we have to construct the unitary time-evolution operator  $U(t, 0)$  which effectuates the propagation of any initial state  $|\psi(0)\rangle$  in time [43],

$$|\psi(t)\rangle = U(t, 0) |\psi(0)\rangle. \quad (27)$$

This operator  $U(t, 0)$  itself obeys the Schrödinger-like equation

$$i\hbar \frac{d}{dt} U(t, 0) = H(t) U(t, 0) \quad (28)$$

with the initial condition

$$U(0, 0) = \text{id}, \quad (29)$$

where  $\text{id}$  denotes the identity operator on  $\mathcal{H}$ . For any Hamiltonian  $H(t)$  the time-evolution operator has the physically transparent semigroup property

$$U(t_1 + t_2, 0) = U(t_1 + t_2, t_1) U(t_1, 0). \quad (30)$$

But in the particular case of a periodically time-dependent Hamiltonian (25) one has even more:

**Assertion 1.** If the Hamiltonian  $H(t) = H(t + T)$  is periodic in time with period  $T$ , the associated time-evolution operator  $U(t, 0)$  obeys the identity

$$U(t + T, 0) = U(t, 0) U(T, 0). \quad (31)$$

This says that knowledge of  $U(t, 0)$  for  $0 \leq t \leq T$  suffices to construct  $U(t, 0)$  for all times  $t \geq 0$ . Although this statement may appear ‘somewhat obvious’, it still needs to be proven. Fortunately, this is not difficult: consider the composite operator

$$V(t) := U(t + T, 0) U^{-1}(T, 0). \quad (32)$$

Then, obviously, one has both

$$V(0) = \text{id} = U(0, 0) \quad (33)$$

and

$$\begin{aligned} i\hbar \frac{d}{dt} V(t) &= i\hbar \frac{d}{dt} U(t+T, 0) U^{-1}(T, 0) \\ &= H(t+T) U(t+T, 0) U^{-1}(T, 0) \\ &= H(t) V(t). \end{aligned} \quad (34)$$

Thus,  $U(t, 0)$  and  $V(t)$  obey the same differential equation with the same initial condition, and therefore coincide, which proves the assertion.  $\square$

In the following we restrict ourselves temporarily to systems with a finite-dimensional Hilbert space  $\mathcal{H}$ ; this restriction eliminates certain technical subtleties which will be discussed later with the help of a simple example. Just as the translation operator by a lattice vector plays a prominent role in solid-state physics, it is intuitively clear that the one-cycle evolution operator  $U(T, 0)$ , which is also known as monodromy operator in the mathematical literature [44], must be of particular importance here. We write this one-cycle evolution operator as an exponential in the suggestive form

$$U(T, 0) = \exp(-iGT/\hbar), \quad (35)$$

where the operator  $G$  is Hermitian, possessing real eigenvalues: This makes sure that  $\exp(-iGT/\hbar)$  is unitary, so that all its eigenvalues lie on the unit circle. With the help of this exponential we now define a further unitary operator:

$$P(t) := U(t, 0) \exp(+iGt/\hbar). \quad (36)$$

Then one deduces

$$\begin{aligned} P(t+T) &= U(t+T, 0) \exp(+iG(t+T)/\hbar) \\ &= U(t, 0) (U(T, 0) \exp(+iGT/\hbar)) \exp(+iGt/\hbar) \\ &= P(t), \end{aligned} \quad (37)$$

where the basic assertion (31) has been used in the first step, and the definition (36) in the second. Thus, we can formulate a second important insight:

**Assertion 2.** Under the propositions specified above, the time-evolution operator  $U(t, 0)$  of a  $T$ -periodically time-dependent quantum system has the form

$$U(t, 0) = P(t) \exp(-iGt/\hbar), \quad (38)$$

where the unitary operator  $P(t) = P(t+T)$  is  $T$ -periodic, and the operator  $G$  is Hermitian.  $\square$

Writing the set of eigenvalues of  $U(T, 0) = \exp(-iGT/\hbar)$  as  $\{e^{-i\varepsilon_n T/\hbar}\}$ , and its eigenstates as  $\{|n\rangle\}$ , we have a spectral representation

$$U(T, 0) = \sum_n |n\rangle e^{-i\varepsilon_n T/\hbar} \langle n|, \quad (39)$$

implying

$$e^{-iGt/\hbar} |n\rangle = e^{-i\varepsilon_n t/\hbar} |n\rangle. \quad (40)$$

Now we are in a position to monitor the time-evolution of an arbitrary initial state  $|\psi(0)\rangle$ : Expanding with respect to the

eigenstates of  $U(T, 0)$ , we start with

$$\begin{aligned} |\psi(0)\rangle &= \sum_n |n\rangle \langle n| \psi(0)\rangle \\ &= \sum_n a_n |n\rangle, \end{aligned} \quad (41)$$

where  $a_n = \langle n|\psi(0)\rangle$ . Applying  $U(t, 0)$ , we then find

$$\begin{aligned} |\psi(t)\rangle &= U(t, 0) |\psi(0)\rangle \\ &= \sum_n a_n P(t) e^{-iGt/\hbar} |n\rangle \\ &= \sum_n a_n P(t) |n\rangle e^{-i\varepsilon_n t/\hbar} \\ &= \sum_n a_n |u_n(t)\rangle e^{-i\varepsilon_n t/\hbar}. \end{aligned} \quad (42)$$

In the last step made here we have *defined* the Floquet functions

$$|u_n(t)\rangle := P(t) |n\rangle, \quad (43)$$

which, as a consequence of the identity (37), are  $T$ -periodic:

$$|u_n(t)\rangle = |u_n(t+T)\rangle. \quad (44)$$

For the sake of definite nomenclature we will refer to the states

$$|\psi_n(t)\rangle = |u_n(t)\rangle e^{-i\varepsilon_n t/\hbar} \quad (45)$$

as *Floquet states*; note that these states, in contrast to the  $T$ -periodic Floquet functions  $|u_n(t)\rangle$ , are solutions to the time-dependent Schrödinger equation (26). Since the normalized eigenfunctions  $\{|n\rangle\}$  of  $U(T, 0)$  form a complete set, and  $P(t)$  is unitary, so do the Floquet functions (43) at each instant  $t$ . Thus, we can formulate the content of equation (42) as follows:

**Assertion 3.** Under the propositions specified above, any solution  $|\psi(t)\rangle$  to the time-dependent Schrödinger equation (26) with a  $T$ -periodic Hamiltonian  $H(t)$  can be expanded with respect to the Floquet states,

$$|\psi(t)\rangle = \sum_n a_n |u_n(t)\rangle e^{-i\varepsilon_n t/\hbar}, \quad (46)$$

where the coefficients  $a_n$  do *not* depend on time.  $\square$

The last half-sentence is of central importance for countless applications of this Floquet picture: since the periodic time-dependence is already incorporated into the basis, the expansion coefficients remain constant. This implies that one can assign occupation probabilities  $|a_n|^2$  to the Floquet states which are preserved despite the action of the time-periodic influence, so that several concepts and techniques used for time-independent quantum systems can be carried over to periodically time-dependent ones. Indeed, the phase factors  $e^{-i\varepsilon_n t/\hbar}$  showing up in this expansion (46) resemble the factors  $e^{-iE_n t/\hbar}$  which accompany the time-evolution of energy eigenstates with energies  $E_n$  if their Hamiltonian does not depend on time: the quantities  $\varepsilon_n$  look as if they were energies, and therefore are aptly named *quasienergies*; this designation appears to have been coined in 1966 almost simultaneously by the eminent Soviet physicists Yakov

Borisovich Zel'dovich [36] and Vladimir Ivanovich Ritus [37].

### 3.2. The Brillouin-zone structure of the quasienergy spectrum

In a formal sense, it seems tempting to interpret the preceding considerations as follows: perform the unitary transformation

$$|\psi(t)\rangle = P(t)|\tilde{\psi}(t)\rangle, \quad (47)$$

so that

$$i\hbar\frac{d}{dt}|\psi(t)\rangle = i\hbar\dot{P}(t)|\tilde{\psi}(t)\rangle + P(t)i\hbar\frac{d}{dt}|\tilde{\psi}(t)\rangle, \quad (48)$$

where the overdot means differentiation with respect to  $t$ .

Now the definition (36) implies

$$i\hbar\dot{P}(t) = i\hbar\dot{U}(t)\exp(iGt/\hbar) - U(t)G\exp(iGt/\hbar), \quad (49)$$

giving

$$\begin{aligned} i\hbar\frac{d}{dt}|\psi(t)\rangle &= H(t)U(t)\exp(iGt/\hbar)|\tilde{\psi}(t)\rangle \\ &\quad - U(t)G\exp(iGt/\hbar)|\tilde{\psi}(t)\rangle \\ &\quad + P(t)i\hbar\frac{d}{dt}|\tilde{\psi}(t)\rangle, \end{aligned} \quad (50)$$

where equation (28) has been used. Next, the representation (38) together with the defining equation (47) readily yields

$$U(t)\exp(iGt/\hbar)|\tilde{\psi}(t)\rangle = |\psi(t)\rangle, \quad (51)$$

so that the left-hand side of equation (50) cancels the first term on the right-hand side, leaving us with

$$\begin{aligned} i\hbar\frac{d}{dt}|\tilde{\psi}(t)\rangle &= P^{-1}(t)U(t)\exp(iGt/\hbar)G|\tilde{\psi}(t)\rangle \\ &= G|\tilde{\psi}(t)\rangle. \end{aligned} \quad (52)$$

This looks interesting: the time-independent operator  $G$  here plays the role of the Hamiltonian for the transformed states  $|\tilde{\psi}(t)\rangle$ . Thus, if the transformation (47) corresponds to a change of the frame of reference, it works such that the dynamics, as seen from the new reference frame, are governed by a time-independent Hamiltonian. In fact, this is the guiding principle behind the construction of the Floquet solutions to certain *integrable* periodically time-dependent problems, such as a two-level system in a circularly polarized classical radiation field [45]: in that paradigmatically important example, which will also play a central role for understanding the particular optical-lattice engineering outlined in section 4.5, the Hamiltonian takes the form

$$H_c(t) = \frac{\hbar\omega_0}{2}\sigma_z + \frac{\mu F}{2}(\sigma_x \cos \omega t + \sigma_y \sin \omega t), \quad (53)$$

where  $\sigma_{x,y,z}$  are the usual Pauli matrices [43], and  $\omega_0$  denotes the frequency of a transition between the two states of the undriven system  $H_0 = \hbar\omega_0\sigma_z/2$ . The parameters  $F$  and  $\omega$  specify, respectively, the strength and the frequency of the driving force, and  $\mu$  is the dipole matrix element connecting the two eigenstates of  $H_0$ . Then the transformation (47) is

designed such that it brings us to a frame of reference which co-rotates with the circularly polarized field:<sup>1</sup>

$$P(t) = \exp(i\omega t(\mathbf{1} - \sigma_z)/2), \quad (54)$$

where  $\mathbf{1}$  is the  $2 \times 2$  unit matrix. Evidently, when viewed from the co-rotating frame, the circularly polarized field must appear as a time-independent one. Indeed, working out the transformation

$$\begin{aligned} P^\dagger(t) &\left( H_c(t) - i\hbar\frac{d}{dt} \right) P(t) \\ &= \frac{\hbar\omega}{2}\mathbf{1} + \frac{\hbar}{2}(\omega_0 - \omega)\sigma_z + \frac{\mu F}{2}\sigma_x - i\hbar\frac{d}{dt} \end{aligned} \quad (55)$$

allows one to identify the desired time-independent operator

$$G_c = \frac{\hbar\omega}{2}\mathbf{1} + \frac{\hbar}{2}(\omega_0 - \omega)\sigma_z + \frac{\mu F}{2}\sigma_x, \quad (56)$$

which, upon diagonalization, yields the quasienergies

$$\varepsilon_\pm = \frac{\hbar}{2}(\omega \pm \Omega) \quad (57)$$

with the generalized Rabi frequency

$$\Omega = \sqrt{(\omega_0 - \omega)^2 + (\mu F/\hbar)^2}. \quad (58)$$

Moreover, transforming the eigenstates of  $G_c$  back to the laboratory frame provides the Floquet states of the system (53). These results are also useful in an approximate sense when the driving field is linearly polarized, rather than circularly, so that the Hamiltonian reads

$$H_l(t) = \frac{\hbar\omega_0}{2}\sigma_z + \mu F\sigma_x \cos \omega t. \quad (59)$$

Now the linearly polarized field may be regarded as a superposition of two circularly polarized components with opposite sense of rotation. If one transforms to a frame co-rotating with one of these components, that component appears stationary, whereas the other, counter-rotating component acquires twice its original frequency. Formally this is expressed as

$$\begin{aligned} P^\dagger(t) &\left( H_l(t) - i\hbar\frac{d}{dt} \right) P(t) \\ &= G_c - i\hbar\frac{d}{dt} + \frac{\mu F}{2}(\sigma_x \cos 2\omega t - \sigma_y \sin 2\omega t), \end{aligned} \quad (60)$$

where the transformation  $P(t)$  again is given by equation (54). If one now neglects the double-frequency counter-rotating component, hoping that its effects will average out, quasienergies and Floquet states of the linearly forced two-level system (59) again are provided by the operator (56). This is the famous *rotating-wave approximation* (RWA), which obviously constitutes a particular high-frequency approximation [46].

To give another example of an integrable periodically time-dependent system which can be solved by means of a transformation (47) we mention the linearly forced harmonic

<sup>1</sup> The transformation to the co-rotating frame is already achieved by the operator  $\exp(-i\omega t\sigma_z/2)$ . The additional factor  $\exp(i\omega t/2)\mathbf{1}$  is incorporated here to ensure the required periodicity (37).

oscillator: here the Floquet states are found by transforming to a reference frame attached to an oscillating periodic solution to the corresponding classical equation of motion [47, 48]. But in general, the remarkable equation (52) appears to good to be true. So where is the catch?

A first piece of the answer already appears when taking the limit of the quasienergies (57) for vanishing driving amplitude,  $\mu F/(\hbar\omega) \rightarrow 0$ : then these quasienergies do *not* reduce to the energy eigenvalues  $\pm\hbar\omega_0/2$  of the undriven two-level system. Instead, one has to distinguish two cases: if  $\omega < \omega_0$ , so that the driving frequency is detuned to the red side of the transition, one finds

$$\begin{aligned}\varepsilon_+ &\rightarrow +\hbar\omega_0/2 \\ \varepsilon_- &\rightarrow -\hbar\omega_0/2 + \hbar\omega.\end{aligned}\quad (61)$$

On the other hand, if the driving frequency is blue-detuned, meaning  $\omega > \omega_0$ , one has

$$\begin{aligned}\varepsilon_+ &\rightarrow -\hbar\omega_0/2 + \hbar\omega \\ \varepsilon_- &\rightarrow +\hbar\omega_0/2.\end{aligned}\quad (62)$$

In either case, what does the additional  $+\hbar\omega$  mean?

As the alert reader will have noted when following the general reasoning in the previous section 3.1, the *Floquet multipliers*  $\{e^{-i\varepsilon_n T/\hbar}\}$  are well defined, being the eigenvalues of the one-cycle evolution operator  $U(T, 0)$ . However, these quantities are just complex numbers on the unit circle which have been parametrized in this particular manner to enforce the suggestive form (45) of the fundamental Floquet solutions, but they do not uniquely determine the quasienergies  $\varepsilon_n$ : The complex logarithm, which is needed to extract these quasienergies from the Floquet multipliers, is multi-valued. Since  $e^z = e^{z+m2\pi i}$ , where  $m = 0, \pm 1, \pm 2, \dots$  is an arbitrary integer, the Floquet multipliers thus fix the quasienergies only up to an integer multiple of  $2\pi\hbar/T$ . Introducing the angular frequency

$$\omega = \frac{2\pi}{T}, \quad (63)$$

a quasienergy, labeled by the state index  $n$ , should therefore be regarded as an entire *class*

$$\varepsilon_{(n,m)} := \varepsilon_n + m\hbar\omega; \quad m = 0, \pm 1, \pm 2, \dots \quad (64)$$

of *equivalent representatives*, where  $\varepsilon_n = \varepsilon_{(n,0)}$  has to be selected by some suitable convention; according to equation (64), the quasienergy representative labeled  $(n, m)$  then differs from that  $\varepsilon_n$  by  $m\hbar\omega$ . For instance,  $\varepsilon_n$  might be that representative which falls into the *first quasienergy Brillouin zone*  $-\hbar\omega/2 < \varepsilon \leq +\hbar\omega/2$ , but sometimes other choices are more useful, as in the example discussed in the following section 3.3. This notion of a quasienergy Brillouin zone emphasizes the solid-state analogy: just as a quasimomentum of a particle in a periodic potential  $V(x) = V(x + a)$  is determined only up to  $\hbar$  times an integer multiple of the reciprocal lattice ‘vector’  $2\pi/a$ , a quasienergy of a system governed by a  $T$ -periodic Hamiltonian  $H(t) = H(t + T)$  is determined only up to an integer multiple of the ‘photon’ energy  $\hbar\omega$ .

Hence, the previous result (57) for the quasienergies of a driven two-level system should be written more carefully as

$$\varepsilon_{\pm} = \frac{\hbar}{2}(\omega \pm \Omega) \quad \text{mod } \hbar\omega, \quad (65)$$

thus resolving the question posed after inspecting the limits (61) and (62). Returning to the general case, a well-meant attempt to go beyond equation (39) and to ‘define’ an operator  $G$  acting on the same Hilbert space  $\mathcal{H}$  as the system’s Hamiltonian  $H(t)$  according to

$$‘G = \sum_n |n\rangle \varepsilon_n \langle n|’ \quad (66)$$

would be incomplete without an additional specification, either explicit or implicit, how to resolve the multi-valuedness of each individual  $\varepsilon_n$ . What is more, in many cases it is not even desirable to single out one particular representative of a quasienergy class (64), because it is precisely the ‘mod  $\hbar\omega$ -indeterminacy’ which allows for a physically most transparent description of multiphoton transitions induced by a periodic drive.

### 3.3. Case study: ac-Stark shifts and multiphoton resonances

In order to illustrate this important fact, and thereby to prepare the discussion of the physics occurring in driven optical lattices, we now undertake a small digression and consider the seemingly simple model of a ‘periodically driven particle in a box’ [49], which also prompts us to address some practical issues relevant for numerical computation: a particle of mass  $M$  is supposed to move on the  $x$ -axis between hard walls located at  $x = \pm a$ , as modeled by the unperturbed Hamiltonian

$$H_0(x) = \frac{-\hbar^2}{2M} \frac{d^2}{dx^2} + V(x) \quad (67)$$

with the archetypal ‘box’ potential

$$V(x) = \begin{cases} 0, & |x| < a, \\ \infty, & |x| \geq a, \end{cases} \quad (68)$$

which forces the particle’s wave function to vanish at  $x = \pm a$ . Moreover, the particle is subjected to a sinusoidal force with angular frequency  $\omega$  and amplitude  $F_0$ , conforming to the total Hamiltonian

$$H(x, t) = H_0(x) - F_0 x \cos(\omega t). \quad (69)$$

For demonstration purposes we fix the driving frequency such that it is red-detuned by 5% from the dipole-allowed transition between the unperturbed box ground state with energy  $E_1$ , and the first excited state with energy  $E_2 = 4E_1$ :

$$\hbar\omega = 0.95(E_2 - E_1). \quad (70)$$

Since the model lives in an infinite-dimensional Hilbert space  $\mathcal{H}$ , it is actually *not* fully covered by the mathematical assertions formulated in section 3.1. But since the energies  $E_n$  of the unperturbed box states  $\varphi_n(x)$  grow quadratically with

their quantum number  $n$ ,

$$E_n = \frac{\hbar^2 \pi^2}{8M a^2} n^2; \quad n = 1, 2, 3, \dots, \quad (71)$$

and the dipole matrix element connecting the states  $\varphi_n(x)$  and  $\varphi_m(x)$  falls off quite fast when the difference  $|m - n|$  becomes large,

$$\langle \varphi_m | x | \varphi_n \rangle = \begin{cases} -\frac{16a}{\pi^2} \frac{mn}{(m^2 - n^2)^2}, & m + n \text{ odd} \\ 0, & m + n \text{ even,} \end{cases} \quad (72)$$

it seems reasonable to assume that an external force with the relatively low frequency (70), and with moderate strength, will hardly affect the high-lying states. We therefore truncate the Hilbert space, retaining only the subspace spanned by the  $n_{\max}$  lowest energy eigenstates  $\varphi_n(x)$  of the unperturbed operator (67), and then have to deal with a system of  $n_{\max}$  complex coupled ordinary differential equations which can be integrated numerically by standard routines. In order to calculate the truncated time-evolution matrix  $U(T, 0)$  one takes each of the unperturbed box eigenstates as initial condition,  $\psi_n(x, 0) = \varphi_n(x)$ , and computes the states  $\psi_n(x, T)$  resulting after one period, collecting these state vectors as columns of the monodromy matrix. Finally, diagonalizing this matrix yields the finite-subspace approximations to the Floquet multipliers  $\{e^{-i\varepsilon_n T/\hbar}\}$  as its eigenvalues, and the expansion coefficients of the approximate Floquet functions  $u_n(x, 0)$  as components of its eigenvectors.

Having computed the quasienergy spectrum for suitably chosen  $n_{\max}$ , one faces a problem of visualization: if we were to plot all the  $n_{\max}$  quasienergies obtained from the diagonalization, reduced to the fundamental Brillouin zone, there would be so many data points that one might not be able to recognize the important features, in particular so in cases where  $n_{\max}$  is truly large. In addition, quasienergies resulting from high-lying states close to the ‘truncation border’ might not be converged, and therefore should be left out. But it is not possible to identify quasienergies of such ‘high-lying’ Floquet states by their magnitude, because there exists no ‘quasienergy ordering’ within the Brillouin zone. A useful ordering scheme can be established by considering the squared overlaps  $|\langle \varphi_\ell | n \rangle|^2$  of the eigenvectors  $\{|n\rangle\}$  of the monodromy matrix with the basis states  $\{|\varphi_\ell\rangle\}$ : if one assigns to each state  $|n\rangle$  the index  $\ell_{\max}(n)$  which maximizes that overlap, and then orders the Floquet states and their quasienergies with respect to these indices, one obtains at least a good pre-selection of the desired ‘low-lying’ states.

In figure 3 we display a quasienergy spectrum of the driven particle in the box (69) which has been computed in this manner with  $n_{\max} = 50$  for scaled driving strengths  $0 \leq F_0 a / (\hbar\omega) \leq 10$ , having plotted only quasienergies originating from the 20 lowest box states. The reader who is not already familiar with this kind of plot should dwell a moment to absorb its content: because the driving frequency (70) is slightly red-detuned from the transition between the box eigenstates  $n = 1$  and  $n = 2$ , these two coupled states

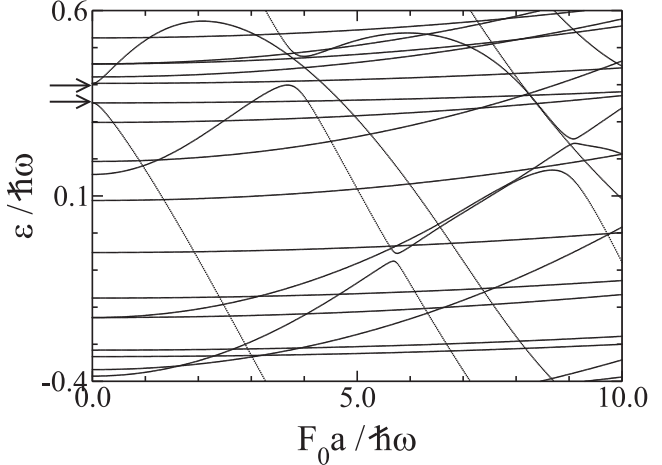


**Figure 3.** One Brillouin zone of quasienergies for the ‘driven particle in a box’ with frequency (70) versus scaled driving amplitude; shown are the quasienergies originating from the 20 lowest box states. Since the unperturbed box eigenstates  $n = 1$  and  $n = 2$  are almost resonant, the quasienergies emanating from these two states, indicated by the arrows, are well described by the RWA-expression (65) in the weak-driving regime  $F_0 a / (\hbar\omega) < 1$ . The Floquet state connected to the unperturbed ground state  $n = 1$  exhibits an almost linear, negative ac-Stark shift even under stronger driving, until it undergoes at  $F_0 a / (\hbar\omega) \approx 4.0$  an avoided crossing with the Floquet state connected to the box state  $n = 3$ . This anticrossing signals the presence of a four-photon resonance. The further avoided crossing at  $F_0 a / (\hbar\omega) \approx 5.7$  indicates a seven-photon resonance, involving the Floquet state emerging from the box state  $n = 4$ .

constitute a two-level system for sufficiently low driving amplitudes. Thus, the quasienergies originating from these two states should conform to equation (65) for weak driving, also assuming the validity of the RWA. Now the difference between red-detuning and blue-detuning shows up: according to equation (61), in the case of a red-detuned driving frequency the quasienergy originating from the upper level is shifted upwards with increasing driving strength, whereas the quasienergy originating from the lower level is shifted downwards. In contrast, equation (62) implies that in case of blue-detuning the quasienergy connected to the lower state would be shifted upwards, while the one connected to the higher state would be shifted downwards (see, e.g., figure 1 in [48]). Such shifts of the quasienergies against the unperturbed energy eigenvalues with increasing driving amplitude are generally known as *ac-Stark shifts*. Indeed, the numerical data shown in figure 3 reveal precisely the expected pattern: the quasienergies emerging from the close-to-resonant unperturbed box eigenstates  $n = 1$  and  $n = 2$ , indicated by the arrows in the left margin, are strongly affected even by weak driving, with the higher state  $n = 2$  exhibiting a positive ac-Stark shift for  $F_0 a / (\hbar\omega) < 1$ , whereas the lower state  $n = 1$  is shifted downwards. For larger driving amplitudes the two-level-RWA naturally breaks down, and the ‘higher’ quasienergy starts to bend, while the ‘lower’ quasienergy is shifted further downwards. If we now properly account for the

Brillouin-zone structure (64) of the quasienergy spectrum and label the quasienergy representatives such that  $\varepsilon_n = \varepsilon_{(n,0)}$  reduces to the energy  $E_n$  of the unperturbed  $n$ th box eigenstate in the limit of vanishing driving strength, the downward-shifted quasienergy representative connected to the unperturbed ground-state energy  $E_1$  in figure 3 carries the label  $(1, 0)$ . When this representative reaches the lower border of the fundamental Brillouin zone, the representative  $(1, 1)$  appears on its upper border, then undergoing a pronounced avoided crossing at  $F_0a/(\hbar\omega) \approx 4.0$  with a quasienergy representative labeled  $(3, -3)$ . It should be no surprise that the quasienergy connected to the ground-state energy of the box is anticrossed from *below*: since there is no quasienergy ordering, the Floquet state originating from the box ground state no longer is a ground state. This anticrossing indicates a strong coupling between the two Floquet states involved, as corresponding to a *multiphoton resonance*.

The close interplay between ac-Stark shifts and multiphoton resonances can be illustrated analytically with the help of the *linearly* polarized two-level system (59): starting from the transformation (60) one obtains the RWA-quasienergies (65) as a first approximation, and then has to account for the counter-rotating terms. These terms have two effects: on the one hand, they cause a further shift of the quasienergies, known as Bloch–Siegert shift. On the other, they couple the two Floquet states when the shifted quasienergies attempt to cross at the boundary of the Brillouin zone, turning the Bloch–Siegert-shifted RWA crossings into avoided crossings (see [50] for a detailed elaboration of this program). Such couplings of two Floquet states, signaled by avoided crossings of their quasienergies, manifest themselves through strongly enhanced long-time averaged transition probabilities under driving with constant amplitude [35].

These resonances constitute one of the most important building blocks for Floquet engineering, and will be put into active use in section 4.6. They also have profound consequences even when the external force is *not* perfectly periodic in time: if one initially populates the box ground state, say, and then subjects the system to a *pulse* with the frequency (70), and with a slowly varying, smooth envelope  $F_0(t)$ , the system's wave function tries to follow the instantaneous Floquet states in an adiabatic manner. However, when encountering an avoided crossing, Landau–Zener-type transitions to the anticrossing state occur [47, 51, 52]. In our example, such adiabatic following combined with Landau–Zener transitions among the anticrossing Floquet states will lead to a partial excitation of the second excited box state  $|\varphi_3\rangle$  after a sufficiently strong pulse. From the difference  $1 - (-3) = 4$  of the respective second entries into the label pairs  $(1, 1)$  and  $(3, -3)$  of the participating quasienergy representatives one deduces that this transition corresponds to a four-photon resonance. In a similar manner, the avoided crossing visible in figure 3 at  $F_0a/(\hbar\omega) \approx 5.7$  indicates a seven-photon resonance, involving quasienergy representatives  $(1, 1)$  and  $(4, -6)$ .

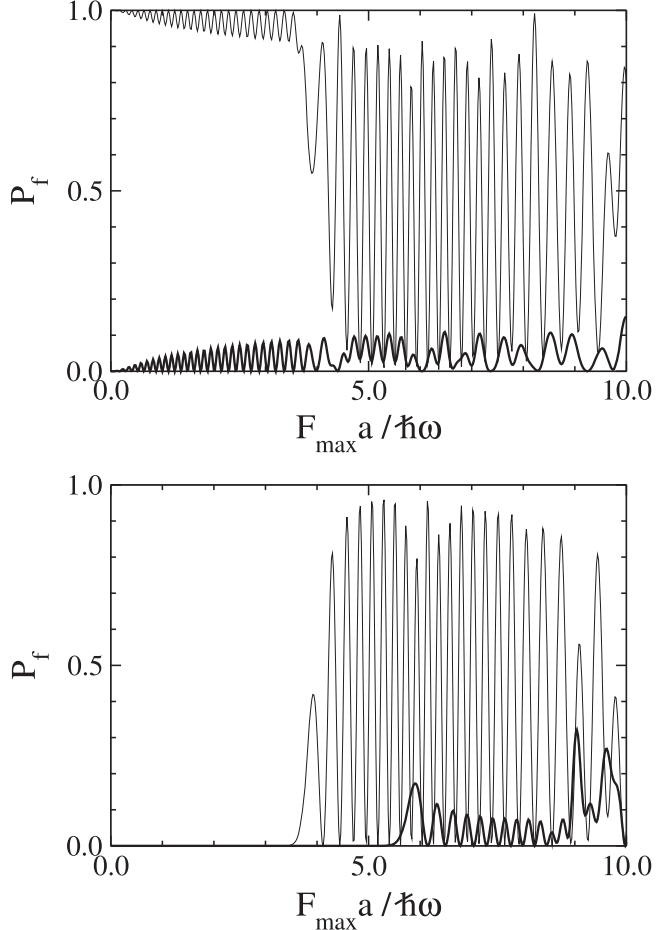


**Figure 4.** Excitation of box eigenstates after Gaussian pulses (73) with width  $\sigma/T = 10$  and near-resonant frequency (70), having started with the ground state  $n = 1$  as initial state. The upper panel shows the final transition probabilities (74) for  $n = 1$  (thin line) and  $n = 2$  (heavy line); the lower panel those for  $n = 3$  (thin line) and  $n = 4$  (heavy line). Observe that these latter states become populated once the pulses are so strong that their envelopes reach the avoided crossings identified in figure 3.

To confirm this quite general scenario, we choose a Gaussian envelope function

$$F_0(t) = F_{\max} \exp\left(-\frac{t^2}{2\sigma^2}\right), \quad (73)$$

start with the box ground state  $\varphi_1(x) = \psi(x, -\infty)$  as initial state, and compute the wave function  $\psi(x, +\infty)$  after the pulse. In figure 4 we show the transition probabilities

$$P_f(n) = |\langle \varphi_n | \psi(+\infty) \rangle|^2 \quad (74)$$

effectuated by such pulses with a width  $\sigma/T = 10$ , as functions of the scaled maximum amplitude. As expected, the second excited box eigenstate  $n = 3$  is significantly populated once the maximum scaled amplitude reaches the large avoided crossing showing up in figure 3 at  $F_0a/(\hbar\omega) \approx 4.0$ ; the third excited state  $n = 4$  appears when the amplitude even reaches the further avoided crossing at  $F_0a/(\hbar\omega) \approx 5.7$ . The oscillating excitation patterns are due to

the fact that the slowly varying envelope traverses the anticrossings twice, during its rise and during its subsequent decrease, so that the two Floquet states which have been populated after the first traversal interfere at the second. This leads to Stueckelberg oscillations, or Ramsey interference fringes. We remark that such oscillations have been detected in experiments with potassium [53] and helium [54] Rydberg atoms driven by short microwave pulses.

### 3.4. The extended Hilbert space

Coming back to the attempt (66) to define an operator  $G$  on  $\mathcal{H}$  by wilfully selecting one particular representative  $\varepsilon_n$  from each class (64), we are faced with a dilemma: which representatives should one pick out in the example depicted in figure 3? Those representatives which connect to the unperturbed box energies in the limit of vanishing driving strength? But then the chosen  $\varepsilon_n$  would not be those representatives which undergo the avoided crossings, while these mark the all-important multiphoton resonances. Or should one take representatives coupled at an avoided crossing? Apart from the fact that this would lead to assignment problems when multiple avoided crossings appear, such representatives would not end up at the unperturbed energy eigenvalues, which appears strange in the perturbative regime of small driving amplitudes. Thus, with the exception of sufficiently simple systems for which there exists a ‘canonical’ choice of quasienergy representatives, it seems advisable to abandon the attempt (66) altogether and to formulate the theory in an invariant manner, such that unnatural distinctions of individual quasienergy representatives are not made. Is this possible?

It is. By inserting the Floquet states (45) into the Schrödinger equation (26) one easily confirms that the Floquet functions  $|u_n(t)\rangle$  satisfy the identity

$$K|u_n(t)\rangle = \varepsilon_n|u_n(t)\rangle, \quad (75)$$

where we have introduced the quasienergy operator

$$K = H(t) - i\hbar \frac{d}{dt}. \quad (76)$$

If at this point the time  $t$  no longer is regarded as the evolution variable, but rather as a *coordinate* on the same footing as  $x$ , this equation (75) becomes an eigenvalue equation in an *extended Hilbert space* of  $T$ -periodic functions, denoted  $L_2[0, T] \otimes \mathcal{H}$ , where  $\mathcal{H}$  is the space that  $H(t)$  acts on, as before. Now, taking one particular  $T$ -periodic solution  $|u_n(t)\rangle$  to equation (75) with eigenvalue  $\varepsilon_n$ , and multiplying by  $e^{im\omega t}$ , where  $\omega$  is given by equation (63) and  $m = 0, \pm 1, \pm 2, \dots$ , the product  $|u_n(t)\rangle e^{im\omega t}$  again is  $T$ -periodic, obeying

$$K|u_n(t)\rangle e^{im\omega t} = (\varepsilon_n + m\hbar\omega)|u_n(t)\rangle e^{im\omega t}. \quad (77)$$

That is, all the quasienergy representatives of a given class (64) appear as individual solutions to this eigenvalue equation (75) in  $L_2[0, T] \otimes \mathcal{H}$ . But they all lead to the *same*

Floquet state (45) in  $\mathcal{H}$ , since

$$\begin{aligned} & (|u_n(t)\rangle e^{im\omega t}) \exp(-i[\varepsilon_n + m\hbar\omega]t/\hbar) \\ & = |u_n(t)\rangle e^{-i\varepsilon_n t/\hbar}, \end{aligned} \quad (78)$$

so that the ‘mod  $\hbar\omega$ -indeterminacy’ drops out.

The extended Hilbert space appears to have been introduced into the physics literature by Hideo Sambe [38]; it plays a major role in the rigorous mathematical analysis of periodically time-dependent quantum systems [55–58]. To fully appreciate what is going on here it is helpful to make another digression and to consider a classical system defined by some explicitly time-dependent Hamiltonian function  $H_{\text{cl}}(p, x, t)$ , giving rise to the Hamiltonian equations

$$\begin{aligned} \frac{dx}{dt} &= \frac{\partial H_{\text{cl}}}{\partial p}, \\ \frac{dp}{dt} &= -\frac{\partial H_{\text{cl}}}{\partial x}. \end{aligned} \quad (79)$$

If one wishes to treat this time-dependent system in analogy to an autonomous one, one regards the time  $t$  as a coordinate, which then naturally possesses a canonically conjugate momentum variable  $p_t$ , leading to an extended phase space  $\{(p, p_t, x, t)\}$ . Next, taking the function

$$K_{\text{cl}}(p, p_t, x, t) = H_{\text{cl}}(p, x, t) + p_t \quad (80)$$

as a Hamiltonian in this extended phase space, one needs an evolution variable which parametrizes the flow it generates; let us denote this evolution variable by  $\tau$ . One then is led to the augmented Hamiltonian system

$$\begin{aligned} \frac{dx}{d\tau} &= \frac{\partial K_{\text{cl}}}{\partial p} = \frac{\partial H_{\text{cl}}}{\partial p}, \\ \frac{dt}{d\tau} &= \frac{\partial K_{\text{cl}}}{\partial p_t} = 1, \\ \frac{dp}{d\tau} &= -\frac{\partial K_{\text{cl}}}{\partial x} = -\frac{\partial H_{\text{cl}}}{\partial x}, \\ \frac{dp_t}{d\tau} &= -\frac{\partial K_{\text{cl}}}{\partial t}, \end{aligned} \quad (81)$$

revealing the close connection of this extended, but autonomous problem to the original one: the second of these equations (81) tells us that the artificial evolution variable  $\tau$  coincides with  $t$ , up to an irrelevant constant which may be taken to be zero. The first and the third equation then reproduce the original system (79), while the fourth one makes sure that the ‘Kamiltonian’ (80) is conserved, as it should, because it does not depend on the time  $\tau$ —recall that  $t$  has been promoted to a coordinate! The use of these extended-phase space techniques allows one, among others, to adapt the semiclassical Einstein–Brillouin–Keller quantization rules for energy eigenstates such that they lend themselves to a semiclassical determination of Floquet states and their quasienergies [59].

Obviously the quasienergy operator (76), acting on the extended Hilbert space  $L_2[0, T] \otimes \mathcal{H}$ , is precisely the quantum counterpart of the augmented Hamiltonian function (80) on the extended phase space, with the classical

‘time-momentum’  $p_t$  having been replaced by the momentum operator (*sic!*)

$$p_t = \frac{\hbar}{i} \frac{d}{dt}; \quad (82)$$

observe that the periodic boundary condition in  $t$  makes sure that this operator is Hermitian. The noteworthy fact that this momentum operator (82) enters only *linearly* into the quasienergy operator  $K$  is responsible for the fact that the spectrum of  $K$ , consisting of all representatives of all quasienergies, is unbounded from below; a property which appears quite unusual in nonrelativistic quantum mechanics. Notwithstanding this technically difficult feature, the eigenvalue equation (75) now plays the role of a *stationary* Schrödinger equation [38].

This recognition leads us to a further element of the Floquet picture: what, then, would be the analog of the time-dependent Schrödinger equation in the extended Hilbert space? The answer to this question is suggested by the classical construction (81): with  $t$  being a coordinate, we require a new evolution variable  $\tau$ , and thus consider states  $|\Psi(\tau, t)\rangle\rangle$ , where, following Sambe [38], the double bracket symbol is meant to indicate that these states reside in  $L_2[0, T] \otimes \mathcal{H}$ , rather than in  $\mathcal{H}$ . For consistency, these states then should obey the Schrödinger-like evolution equation

$$i\hbar \frac{d}{d\tau} |\Psi(\tau, t)\rangle\rangle = K |\Psi(\tau, t)\rangle\rangle. \quad (83)$$

Moreover, in analogy to the classical procedure the actual physical state  $|\psi(t)\rangle$  in  $\mathcal{H}$  should be recovered from  $|\Psi(\tau, t)\rangle\rangle$  by equating  $\tau$  and  $t$ :

$$|\psi(t)\rangle = |\Psi(\tau, t)\rangle\rangle|_{\tau=t}. \quad (84)$$

Indeed, this requirement gives

$$\begin{aligned} i\hbar \frac{d}{dt} |\psi(t)\rangle &= i\hbar \frac{d}{d\tau} |\Psi(\tau, t)\rangle\rangle|_{\tau=t} + i\hbar \frac{d}{dt} |\Psi(\tau, t)\rangle\rangle|_{\tau=t} \\ &= \left( H(t) - i\hbar \frac{d}{dt} \right) |\Psi(\tau, t)\rangle\rangle|_{\tau=t} \\ &\quad + i\hbar \frac{d}{dt} |\Psi(\tau, t)\rangle\rangle|_{\tau=t} \\ &= H(t) |\psi(t)\rangle, \end{aligned} \quad (85)$$

where equation (83) has been used in the second step, together with the definition (76) of the quasienergy operator  $K$ : the evolution equation (83) in  $L_2[0, T] \otimes \mathcal{H}$ , together with the prescription (84) for ‘projecting back’ from  $L_2[0, T] \otimes \mathcal{H}$  to the physical Hilbert space  $\mathcal{H}$ , implies the correct Schrödinger equation (26). This suggests that the states  $|\psi(t)\rangle$  of a periodically time-dependent quantum system may be regarded as ‘projection shadows’, in the sense of equation (84), of larger objects which are governed by a ‘Kamiltonian’ involving a momentum operator only to its first power. This is what makes these systems so exciting, both literally and metaphorically speaking, and this is what underlies much of their potential for quantum engineering.

The evolution equation (83) provides the key for establishing an adiabatic principle for Floquet states [47, 51, 52, 60], for connecting multiphoton transitions, as exemplified in figure 4, to Landau–Zener transitions among Floquet states [47, 51, 52], and for superadiabatic Floquet analysis [52]. But is there also something more tangible, beyond formal consistency?

There is. The traditionally trained reader may have been severely worried by figure 4: the unperturbed box Hamiltonian (67) is invariant under the reflection  $x \rightarrow -x$ , so that its eigenfunctions  $\varphi_n(x)$  possess the definite parity  $(-1)^{n+1}$ . Moreover, the dipole operator  $x$  which mediates the time-periodic perturbation according to equation (69) only connects states with different parity, meaning that all dipole matrix elements (72) between states of equal parity vanish. Hence, the transition from  $n = 1$  to  $n = 2$  is ‘dipole-allowed’, whereas the transition from  $n = 1$  to  $n = 3$  is ‘dipole-forbidden’—in apparent contradiction to the numerical results shown in figure 4. Even more, the occupation of the seemingly favored final state  $n = 2$  would actually be adiabatically suppressed if the pulses were made longer. What is happening here?

The answer to this pertinent question, of course, lies in the observation that the reflection symmetry only refers to the unperturbed system (67), and therefore remains meaningful as long as the driving force remains ‘perturbatively weak’. But if this is no longer the case, because the dimensionless quantity  $F_0 a / (\hbar\omega)$  is taken to be on the order of unity or larger, then it is not the symmetry of  $H_0$  in  $\mathcal{H}$  which matters, but rather that of  $K$  in  $L_2[0, T] \otimes \mathcal{H}$ . Now the quasienergy operator (76) constructed from the full Hamiltonian (69) remains invariant under the spatio-temporal transformation

$$P : \begin{cases} x \rightarrow -x \\ t \rightarrow t + T/2; \end{cases} \quad (86)$$

since  $P^2 = \text{id}$  (keeping in mind that  $t + T$  equals  $t$  in  $L_2[0, T] \otimes \mathcal{H}$ ) the eigenfunctions of  $K$  acquire a definite sign under this generalized parity operation. Assuming the same labeling as before, so that the quasienergy representative  $(n, 0)$  connects to the unperturbed box energy  $E_n$  in the limit of vanishing driving strength, one finds that a representative labeled  $(n, m)$  is associated with the generalized parity  $(-1)^{n+m+1}$ —for a proof, consider the particular parameter  $F_0 a / (\hbar\omega) = 0$ , for which the Floquet functions coincide with the unperturbed box eigenfunctions, times  $e^{im\omega t}$ . Now there is the famous von Neumann–Wigner noncrossing rule: eigenvalues of a Hermitian operator do not cross if only one single parameter is varied, unless there is a symmetry which allows such crossings [61]. Applied to the quasienergy spectrum of the periodically driven particle in the box, as displayed in figure 3, this means that quasienergy representatives possessing the same generalized parity are not allowed to cross upon variation of  $F_0 a / (\hbar\omega)$ , and therefore produce multiphoton resonances, whereas representatives having different generalized parities do not ‘feel’ each other and may cross. Indeed, the representatives  $(1, 1)$  and  $(3, -3)$  repelling each other and thereby effectuating the four-photon-resonance located at  $F_0 a / (\hbar\omega) \approx 4.0$  both fall into the same generalized parity

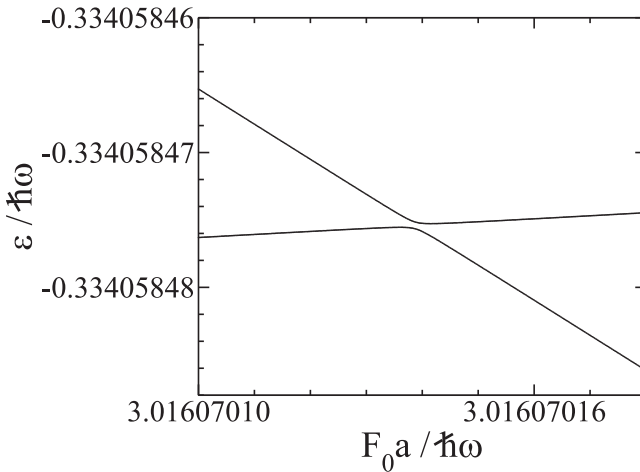


**Figure 5.** Magnified detail of figure 3, showing an anticrossing between quasienergy representatives  $(1, 0)$  and  $(6, -13)$ . Almost needless to stress: observe the scales!

class, as do the representatives  $(1, 1)$  and  $(4, -6)$  which form the seven-photon resonance at  $F_0 a / (\hbar\omega) \approx 5.7$ . Thus, the concept of the extended Hilbert space is essential for understanding nonperturbative excitation patterns.

### 3.5. Coarse graining

Taking the noncrossing rule seriously, about half of the apparent crossings observed in figure 3 actually should be nonresolved anticrossings. This is exemplified by figure 5, which shows a magnification of a detail far below the resolution of figure 3, namely, the expected anticrossing of the quasienergy representatives  $(1, 0)$  and  $(6, -13)$ , corresponding to an extremely narrow 13-photon resonance. In a similar manner one confirms the validity of the noncrossing rule at other instances, although it becomes hard to maintain the required numerical accuracy at high-order resonances.

But now we have opened Pandora's box. Recall that each of the infinitely many box eigenstates plants one quasienergy representative into the fundamental Brillouin zone, so that, at least for a generic choice of the driving frequency, the quasienergy spectrum will be 'dense' already for  $F_0 a / (\hbar\omega) = 0$ . If the previously constructed picture, resulting from finite-subspace approximations, actually still holds water even when considering the full infinite-dimensional system, this would imply infinitely many anticrossings 'on arbitrarily small scales' within an arbitrarily small interval of the scaled driving strength; hence, it seems unlikely that the 'true' quasienergies are differentiable. There are resonances virtually everywhere—although the vast majority of them evidently have to be of *very* high order, such that they should not matter much.

At this point, the attitudes of mathematicians and physicists may differ. The mathematician will observe that, when studying systems like the driven particle in the box (69), one is dealing with the problem of the perturbation of a dense point spectrum, which is far from trivial. In particular, one may pose the question whether there exists a transition from a

dense pure point spectrum to an absolutely continuous one at a certain nonzero driving strength [42]. While a dense point quasienergy spectrum gives rise to quasiperiodic motion [62], a continuous quasienergy spectrum would lead to diffusive energy growth [63]; the question under what conditions there can be a transition from one type of motion to the other constitutes the content of the so-called *quantum stability problem* [42, 64]. This problem has been studied in great depth for the model of the 'δ-kicked rotator' [65]: while its quasienergy spectrum has a continuous component when the frequency of the kicks is rationally related to the frequencies of the free rotator [66], it is pure point otherwise [42]. Eminent contributions to the general subject of quantum stability have been made by James Howland, who has established conditions guaranteeing the absence of an absolutely continuous spectrum [42, 56]. Using these, it has been shown that linearly driven anharmonic oscillators with a superquadratic potential, such as the driven particle in a box, are 'stable' in this sense [57].

The physicist, on the other hand, may feel that a mathematical model like that given by equation (69) provides only a limited description of some larger, experimentally accessible system, so that it might not always be meaningful to solve such a restricted model on a level at which it no longer applies. To be definite, a tiny avoided quasienergy crossing of width  $\delta\epsilon$ , such as shown in figure 5, is associated with a large time scale on the order of  $\hbar/\delta\epsilon$ , and would not be detectable in shorter measurements. In experiments with pulses such tiny anticrossings would be traversed in a perfectly diabatic manner and therefore remain hidden, *unless* the time scale characterizing the change of the pulses' envelope matches  $\hbar/\delta\epsilon$ . But then, who could design pulses with 'infinitely slowly' varying envelopes?

Thus, in many cases of experimental interest it may be reasonable to ignore infinitely many quasienergy anticrossings below a certain scale determined by the respective set-up. This 'coarse graining' strategy had automatically been implied by figure 3: the 20 'lowest' quasienergies displayed there actually undergo avoided crossings with 'higher' states which have been omitted, but these anticrossings are too small to be seen, so that the remaining lines appear smooth on the scale of figure 3. That same coarse graining approach, as well as its limitations, will be met again in the following calculations of quasienergy bands for periodically driven optical lattices. If coarse graining is feasible, one may construct an effective time-independent Hamiltonian which describes the dynamics within some restricted subspace [25]; if not, efficient coupling among Floquet states causes heating of the driven system.

On a technical level, coarse graining amounts to constructing an integrable approximation to a near-integrable system. This usually involves some sort of high-frequency approximation for averaging out residual oscillating perturbations, similar to the rotating-wave approximation to the linearly polarized two-level system (59). A systematic discussion of such approximation schemes within the Floquet picture has recently been given in [67]. It might also be worthwhile to point out that the quantum stability problem

still remains virtually unexplored for periodically forced systems comprising many interacting particles: In view of the tremendous density of states resulting from folding their unperturbed energy spectra into the Brillouin zone, it might be hard to find generic driven many-body systems that are truly stable in the sense of [42, 64].

For completeness, we briefly mention another important branch of the theory: When considering, for instance, a hydrogen atom exposed to a monochromatic classical driving force, one is dealing with the perturbation of eigenstates embedded in a continuous spectrum. The resulting Floquet states then are *resonances* with a finite lifetime, as described mathematically by complex poles of the resolvent of the quasienergy operator [68]. This is exploited in practical computations of, e.g., ionization probabilities with the help of complex scaling techniques [41], but these are not required for the present purposes.

#### 4. Floquet engineering with optical lattices

We now turn to the central topic of this tutorial, aiming at the deliberate manipulation, and control, of quantum dynamics in driven optical lattices. Thus, we consider a quantum particle which moves in a spatially periodic potential  $V$  with ‘lattice constant’  $a$ ,

$$V(x) = V(x + a), \quad (87)$$

while it is acted on by a spatially homogeneous, temporally periodic force  $F$  with period  $T$ ,

$$F(t) = F(t + T). \quad (88)$$

Assuming dipole coupling, as for the particle in the box (69), the Hamiltonian takes the form

$$\tilde{H}(x, t) = -\frac{\hbar^2}{2M} \frac{d^2}{dx^2} + V(x) - xF(t), \quad (89)$$

and the task again is to characterize *all* solutions to the time-dependent Schrödinger equation

$$i\hbar \frac{d}{dt} \tilde{\psi}(x, t) = \tilde{H}(x, t) \tilde{\psi}(x, t). \quad (90)$$

We proceed in three steps: in section 4.1 we provide a general formulation of our approach, introducing quasienergy bands and quasienergy dispersion relations. In section 4.2 we then discuss driven optical cosine lattices, and show how their quasienergy dispersion relations are computed in practice, combining the essentials of sections 2 and 3. In the remaining sections 4.3 to 4.6 we then explain specific examples of Floquet engineering, showing how to create quasienergy dispersion relations with certain desired properties. Throughout, we will make heavy use of the theoretical concepts introduced in the previous section 3—the quasienergy Brillouin zone, ac-Stark shifts, multiphoton resonances, the extended Hilbert space, and coarse graining—and demonstrate their experimental implications.

#### 4.1. Spatio-temporal Bloch waves

In order to exploit both the spatial periodicity (87) and the temporal periodicity (88), we perform the unitary transformation

$$\tilde{\psi}(x, t) = \exp \left( \frac{i}{\hbar} x \int_0^t d\tau F(\tau) \right) \psi(x, t) \quad (91)$$

which brings the coupling of the external force to the particle into a different, but quite familiar guise: observing

$$\begin{aligned} i\hbar \frac{d}{dt} \tilde{\psi}(x, t) &= \exp \left( \frac{i}{\hbar} x \int_0^t d\tau F(\tau) \right) \\ &\times \left( i\hbar \frac{d}{dt} \psi(x, t) - xF(t)\psi(x, t) \right) \end{aligned} \quad (92)$$

and invoking the identity (15), we are led to the transformed Schrödinger equation

$$i\hbar \frac{d}{dt} \psi(x, t) = H(x, t) \psi(x, t) \quad (93)$$

with the new Hamiltonian

$$H(x, t) = \frac{1}{2M} \left( p + \int_0^t d\tau F(\tau) \right)^2 + V(x). \quad (94)$$

Here the homogeneous force couples to the particle in the same gauge-invariant manner as a homogeneous electric field would couple to a particle with charge  $e$ : introducing the space-independent ‘vector potential’

$$eA(t) = - \int_0^t d\tau F(\tau), \quad (95)$$

so that

$$F(t) = -e \frac{dA(t)}{dt}, \quad (96)$$

one has

$$H(x, t) = \frac{1}{2M} (p - eA(t))^2 + V(x). \quad (97)$$

But the actual reason for resorting to the transformation (91) lies elsewhere: If we now stipulate that the force does not contain a dc component, so that

$$\frac{1}{T} \int_0^T dt F(t) = 0, \quad (98)$$

this Hamiltonian (94) is periodic in both space and time:

$$H(x, t) = H(x + a, t) = H(x, t + T). \quad (99)$$

Accordingly, we can apply both the common Bloch theory as known from solid-state physics [31, 32], and the Floquet theory outlined in section 3. Hence, a Hamiltonian with the two-fold translational symmetry (99) gives rise to a complete set of spatio-temporal Bloch waves [69–71]

$$\psi_{n,k}(x, t) = \exp [ikx - i\varepsilon_n(k)t/\hbar] u_{n,k}(x, t) \quad (100)$$

characterized simultaneously by a wave number  $k$  and a quasienergy  $\varepsilon_n(k)$ ; as in section 2, an additional index  $n$  is required for distinguishing different *quasienergy bands*. The Bloch–Floquet functions  $u_{n,k}(x, t)$  now embody both

translational symmetries, so that

$$u_{n,k}(x, t) = u_{n,k}(x + a, t) = u_{n,k}(x, t + T). \quad (101)$$

The rationale behind the introduction of these quasienergy bands lies in the fact that they open up far-reaching analogies: a particle in the  $n$ th energy band  $E_n(k)$  of a lattice  $V(x) = V(x + a)$  without driving force  $F(t)$  is described by a wave packet

$$\begin{aligned} \psi_n(x, t) = & \sqrt{\frac{a}{2\pi}} \int dk g_n(k) \\ & \times \exp[ikx - iE_n(k)t/\hbar] u_{n,k}(x) \end{aligned} \quad (102)$$

built from the usual Bloch waves (9), where the integration ranges over one Brillouin zone  $-\pi/a \leq k < \pi/a$  in  $k$ -space. Assuming the  $k$ -space distribution  $g_n(k)$  to be sufficiently smooth, and well centered around its first moment

$$k_c = \int dk k |g_n(k)|^2, \quad (103)$$

the packet's group velocity is given by

$$v_g = \frac{1}{\hbar} \frac{dE_n(k)}{dk} \Big|_{k_c}. \quad (104)$$

Moreover, if an arbitrary, but weak homogeneous force  $f(t)$  acts on the system, such that it does not produce appreciable interband transitions, the moment (103) evolves in time according to the semiclassical 'acceleration theorem' [31]

$$\hbar \frac{dk_c(t)}{dt} = f(t). \quad (105)$$

In complete analogy, a particle prepared in the  $n$ th quasienergy band of a periodically driven lattice is given by a packet [71]

$$\begin{aligned} \psi_n(x, t) = & \sqrt{\frac{a}{2\pi}} \int dk g_n(k) \\ & \times \exp[ikx - i\varepsilon_n(k)t/\hbar] u_{n,k}(x, t) \end{aligned} \quad (106)$$

made up from the spatio-temporal Bloch waves (100), with the occupation amplitudes  $g_n(k)$  remaining *constant* in time, despite the action of the external force. This is an immediate consequence of assertion 3 formulated in section 3.1: while the driving force may give rise to even violent transitions between the unperturbed energy bands, these transitions are incorporated into the spatio-temporal Bloch basis (100), to the effect that the occupation numbers of these time-dependent basis states are preserved in time. In addition, assuming the quasienergy dispersion relation  $\varepsilon_n(k)$  to be sufficiently smooth,<sup>2</sup> the cycle-averaged group velocity of such a packet (106) is determined by its derivative,

$$\bar{v}_g = \frac{1}{\hbar} \frac{d\varepsilon_n(k)}{dk} \Big|_{k_c}. \quad (107)$$

Finally, if the total driving force  $F(t) + f(t)$  consists of a strong time-periodic component  $F(t)$  which creates the

<sup>2</sup> The proposition of sufficient smoothness may not always be satisfied; it requires that coarse graining works reasonably well: see the quasienergy bands displayed in sections 4.3–4.6 !

Floquet states, and an additional weak component  $f(t)$ , one again finds an acceleration theorem of the form (105) [71]. Thus, the introduction of quasienergy dispersion relations  $\varepsilon_n(k)$  allows one to assess the essential dynamics in homogeneously driven lattices in close analogy to the approach taken in energy band-based solid state physics.

Inserting the ansatz (100) into the Schrödinger equation (93), and once again using equation (15), we obtain the quasienergy eigenvalue equation which determines the quasienergy band structure:

$$\begin{aligned} & \left[ \frac{1}{2M} \left( p + \hbar k + \int_0^t d\tau F(\tau) \right)^2 \right. \\ & \left. + V(x) - i\hbar \frac{d}{dt} \right] u_{n,k}(x, t) \\ & = \varepsilon_n(k) u_{n,k}(x, t). \end{aligned} \quad (108)$$

This is the concrete form of the eigenvalue equation (75) required here, defined on the extended Hilbert space  $L_2[0, T] \otimes \mathcal{H}$  which hosts the eigenfunctions  $u_{n,k}(x, t)$ . Viewed from the perspective of this extended Hilbert space, which prompts us, in the sense discussed in section 3.4, to treat the time variable  $t$  as a coordinate on the same footing as  $x$ , a time-periodically driven lattice thus appears as a 'spatio-temporal lattice', with the drive extending the spatial periodicity imposed by the lattice potential  $V$  to the additional 'time coordinate'. Even if the spatial lattice potential  $V$  is kept fixed, one can manipulate the quasienergy dispersion relations  $\varepsilon_n(k)$  of this spatio-temporal lattice by suitably adjusting its temporal component, i.e., the parameters of the driving force. This sets the scope for Floquet engineering of dispersion relations, and opens up a wide field of possibilities far beyond the reach of customary solid-state physics.

In passing, we remark that the 'zero average' condition (98) imposed on the force  $F(t)$  can still be relaxed: quasienergy bands exist when [71]

$$\int_0^T dt F(t) = r \times \hbar \frac{2\pi}{a}; \quad r = 0, \pm 1, \pm 2, \dots \quad (109)$$

For instance, this can be the case when the force is monochromatic with an additional static component. If

$$F(t) = F_r + F_0 \cos(\omega t), \quad (110)$$

the static component  $F_r$  of the force 'tilts' the lattice, leading to the appearance of Wannier–Stark ladders [72, 73], and the equality (109) gives

$$F_r a = r \times \hbar \omega \quad (111)$$

with  $\omega = 2\pi/T$ , requiring that the spacing  $F_r a$  between the rungs of these ladders be equal to the energy of  $r$  'photons'. While situations in which  $r \neq 0$  do possess an intrinsic interest of their own [74, 75], here we restrict ourselves to  $r = 0$ .

The numerical solution of this eigenvalue equation (108) can be accomplished by combining the techniques reviewed in sections 2 and 3. First one chooses a convenient and suitably truncated basis set which incorporates the spatial periodic boundary condition, and fixes a wave number  $k$ . Then

each basis state is propagated in time over one period  $T$ . The propagated states form the columns of the truncated one-cycle evolution matrix  $U_k(T, 0)$ , the diagonalization of which finally yields both the approximate quasienergies  $\varepsilon_n(k)$  (mod  $\hbar\omega$ ), and the approximate expansion coefficients of the Floquet functions  $u_{n,k}(x, 0)$  with respect to the basis used. Repeating this procedure for a sufficiently fine mesh of  $k$ -values gives the desired quasienergy dispersion relations.

#### 4.2. Ultracold atoms in shaken optical lattices

In the particular case of ultracold atoms in an optical cosine lattice, as considered briefly in section 2, the time-periodic force on the electrically neutral particles is generated by exploiting their inertia. For example, one can mount a mirror which retro-reflects a laser beam back into itself, and thus creates the standing wave transforming into the optical lattice potential, onto a piezoelectric actuator, enabling one to ‘shake’ the lattice back and forth [11]. This shaking motion then transforms into an inertial force on the atoms in a frame comoving with the lattice. That is, one starts in the laboratory frame of reference with a Hamiltonian of the form

$$H^{\text{lab}}(x, t) = \frac{p^2}{2M} + \frac{V_0}{2} \cos(2k_L[x - \Delta L \cos(\omega t)]), \quad (112)$$

where  $\Delta L$  denotes the amplitude of shaking, and performs the unitary transformation

$$\psi^{\text{lab}}(x, t) = \exp\left(-\frac{i}{\hbar}\Delta L \cos(\omega t)p\right) \psi^{\text{cm}}(x, t). \quad (113)$$

Since, in analogy to equation (15), one has the identity

$$\begin{aligned} & \exp\left(+\frac{i}{\hbar}\Delta L \cos(\omega t)p\right) x \exp\left(-\frac{i}{\hbar}\Delta L \cos(\omega t)p\right) \\ &= x + \frac{i}{\hbar}\Delta L \cos(\omega t)[p, x] \\ &= x + \Delta L \cos(\omega t), \end{aligned} \quad (114)$$

this brings us to the comoving frame of reference. Moreover, observing that

$$\begin{aligned} i\hbar \frac{d}{dt} \psi^{\text{lab}}(x, t) &= \exp\left(-\frac{i}{\hbar}\Delta L \cos(\omega t)p\right) \\ &\times \left( i\hbar \frac{d}{dt} \psi^{\text{cm}}(x, t) - \Delta L \omega \sin(\omega t)p \psi^{\text{cm}}(x, t) \right), \end{aligned} \quad (115)$$

the Hamiltonian in this latter frame becomes

$$\begin{aligned} H^{\text{cm}}(x, t) &= \frac{p^2}{2M} + \Delta L \omega \sin(\omega t)p + \frac{V_0}{2} \cos(2k_L x) \\ &= \frac{1}{2M}(p + M\Delta L \omega \sin(\omega t))^2 + \frac{V_0}{2} \cos(2k_L x) \\ &\quad - \frac{M}{2}(\Delta L \omega)^2 \sin^2(\omega t), \end{aligned} \quad (116)$$

having completed the square of the momentum in the second step. This comoving-frame Hamiltonian already resembles the previous operator (94), except for its last, merely time-dependent term. It might be tempting to ‘gauge away’ this

additional term by the further unitary transformation

$$\psi^{\text{cm}}(x, t) = \exp\left(\frac{i}{\hbar} \int_0^t d\tau \frac{M}{2}(\Delta L \omega)^2 \sin^2(\omega \tau)\right) \psi(x, t), \quad (117)$$

but this would be against the rules: because of the form (38) of the time-evolution operator  $U(t, 0)$ , a unitary transformation will leave the system’s quasienergy spectrum unaltered only if the transformation itself is  $T$ -periodic. Now the elementary identity

$$\sin^2(\omega t) = \frac{1}{2}(1 - \cos(2\omega t)) \quad (118)$$

implies that the exponential generating the transformation (117) contains a secular contribution which grows linearly in time, spoiling the required  $T$ -periodicity. This deficiency is cured by extracting the secular term: performing the  $T$ -periodic transformation

$$\begin{aligned} \psi^{\text{cm}}(x, t) &= \exp\left(-\frac{i}{\hbar} \int_0^t d\tau \frac{M}{4}(\Delta L \omega)^2 \cos(2\omega \tau)\right) \psi(x, t) \\ &= \exp\left(-\frac{i}{8\hbar} M \Delta L^2 \omega \sin(2\omega t)\right) \psi(x, t), \end{aligned} \quad (119)$$

we find that the wave functions  $\psi(x, t)$  are governed by the Hamiltonian

$$\begin{aligned} H(x, t) &= \frac{1}{2M}(p + M\Delta L \omega \sin(\omega t))^2 \\ &\quad + \frac{V_0}{2} \cos(2k_L x) - \frac{M}{4}(\Delta L \omega)^2. \end{aligned} \quad (120)$$

This corresponds to the previous form (94), involving a sinusoidal force

$$F(t) = F_0 \cos(\omega t) \quad (121)$$

with amplitude

$$F_0 = M\Delta L \omega^2. \quad (122)$$

The additional energy shift appearing in the Hamiltonian (120) possesses an intuitive interpretation: consider a classical particle moving according to Newton’s equation

$$M\ddot{x}(t) = F(t), \quad (123)$$

so that

$$\dot{x}(t) = \frac{F_0}{M\omega} \sin(\omega t), \quad (124)$$

up to a constant. The average ‘quiver energy’ of the particle then is given by

$$\begin{aligned} \frac{1}{2}M\dot{x}^2 &= \frac{F_0^2}{4M\omega^2} \\ &= \frac{M}{4}(\Delta L \omega)^2; \end{aligned} \quad (125)$$

this is the analog of the ‘ponderomotive energy’ known from the study of electrons in intense laser fields [76]. Thus, quasienergy spectra computed for a ‘minimal coupling’ Hamiltonian (94) incorporate the ponderomotive energy,

while those computed for a ‘shaking’ Hamiltonian (112) do not.

We now write the spatio-temporal Bloch waves (100) for a driven optical lattice as

$$\psi_{n,k}(x, t) = e^{ikx} \chi_{n,k}(x, t), \quad (126)$$

so that the Floquet states for given wave number  $k$ ,

$$\chi_{n,k}(x, t) = u_{n,k}(x, t) e^{-i\varepsilon_n(k)t/\hbar}, \quad (127)$$

obey the Schrödinger equation

$$i\hbar \frac{d}{dt} \chi_{n,k}(x, t) = \left[ \frac{1}{2M} \left( p + \hbar k + \frac{F_0}{\omega} \sin(\omega t) \right)^2 + \frac{V_0}{2} \cos(2k_L x) \right] \chi_{n,k}(x, t), \quad (128)$$

referring to the form (94) of the Hamiltonian. We then employ the dimensionless scaled coordinate  $z = k_L x$ , as in section 2, together with the dimensionless time  $\tau = \omega t$ , and eliminate merely time-periodic terms without much ado. Dividing by the recoil energy (4), we arrive at the conveniently scaled equation

$$i\frac{\hbar\omega}{E_R} \frac{d}{d\tau} \chi_{n,k}(z, \tau) = \left[ -\frac{d^2}{dz^2} + \left( \frac{k}{k_L} \right)^2 + \frac{1}{2} \beta^2 + \frac{V_0}{2E_R} \cos(2z) + 2 \left( \frac{k}{k_L} + \beta \sin \tau \right) \frac{1}{i} \frac{d}{dz} \right] \chi_{n,k}(z, \tau) \quad (129)$$

which contains, apart from the reduced wave number  $k/k_L$ , three tunable dimensionless parameters: The scaled lattice depth  $V_0/E_R$ , the scaled driving frequency  $\hbar\omega/E_R$ , and the scaled driving amplitude

$$\beta = \frac{F_0/k_L}{\hbar\omega}. \quad (130)$$

Observe that  $\beta^2/2$  is the ponderomotive energy (125) in units of the recoil energy; this contribution should be left out when working with a ‘shaking lattice’ Hamiltonian (112). An efficient numerical algorithm for computing the quasienergy bands now again employs the trigonometric basis  $\{\varphi_\mu(z); \mu = 0, 1, 2, 3, \dots\}$  given by equations (20) and (21), so that the periodic boundary conditions in space are properly accounted for, and the operators entering into this equation (129) acquire the matrix representations (22), (23), and (24), suitably truncated. The actual computation then proceeds in precise analogy to the example of the driven particle in the box studied in section 3.3: Each basis state  $\varphi_\mu(z)$  is taken as initial condition  $\chi(z, 0)$  for equation (129) and propagated over one period in time, providing the  $\mu$ th column of the monodromy matrix; upon diagonalization, this matrix yields quasienergies and Floquet functions. As shown in the Appendix, the numerical effort can still be reduced by exploiting the symmetries of the quasienergy operator.

**Table 1.** Widths  $W_0$  and  $W_1$  of the lowest two energy bands, and magnitude of the gap  $\Delta_{01}$  between them at  $k/k_L = \pm 1$ , for optical lattices with the depths  $V_0$  considered in figure 2.

$V_0/E_R$	$W_0/E_R$	$\Delta_{01}/E_R$	$W_1/E_R$
4.0	0.345	1.969	2.058
8.0	0.123	3.770	1.293

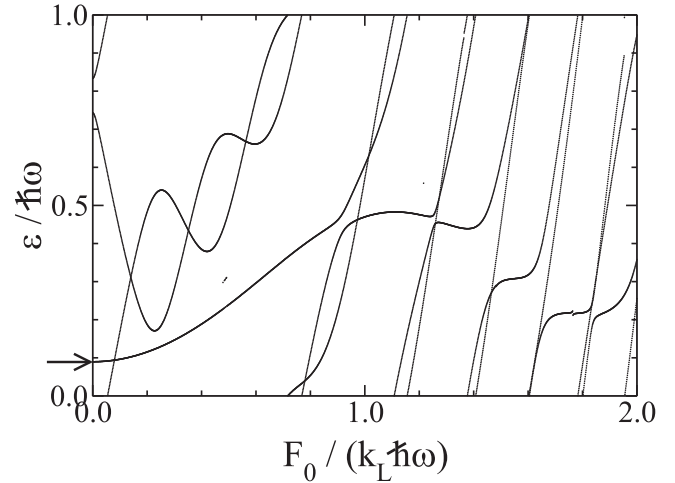


**Figure 6.** Ac-Stark shifts of the edges  $k/k_L = 0$  of the lowest three bands  $n = 0$  (indicated by the arrow),  $n = 1$ , and  $n = 2$  of an optical cosine lattice with depth  $V_0/E_R = 4.0$  in response to a driving force with frequency  $\hbar\omega/E_R = 0.5$ .

#### 4.3. Multiphoton-like resonances in optical lattices

To start the discussion of actual Floquet engineering, and to give some selected examples of the rich variety of quasi-energy dispersion relations that can be realized with driven optical lattices, we again consider cosine potentials with depth  $V_0/E_R = 4.0$  or  $V_0/E_R = 8.0$ , for which the undriven energy dispersion relations had been displayed in figure 2; some relevant figures of merit for these lattices are listed in table 1. For orientation: if one works with atoms of  $^{87}\text{Rb}$  in a lattice generated by laser radiation with wave length  $\lambda = 842$  nm, as in an experiment reported by Zenesini *et al* [11], the recoil frequency  $\nu = E_R/h$  amounts to 3.23 kHz; typical driving frequencies thus fall into the lower kilohertz regime.

In figure 6 we show the ac-Stark shifts of the edges  $k/k_L = 0$  of the lowest three bands of a cosine lattice with depth  $V_0/E_R = 4.0$  in response to a drive applied with the frequency  $\hbar\omega/E_R = 0.5$ , so that the ‘photon’ energy  $\hbar\omega$  is somewhat larger than the width  $W_0$  of the undriven lowest energy band, while the gap  $\Delta_{01}$  between the lowest and the first excited band is roughly equal to  $4 \hbar\omega$ . Despite this gap, the shifting ‘lowest’ band edge, indicated by the arrow, is heavily disrupted by resonances with the shifted higher edges when the driving amplitude (130) reaches the nonperturbative regime. Note that this figure includes the ponderomotive energy, as do all following ones. But still, in order to assess the dynamics of a Floquet wave packet (106) the inspection of states with just one single wave number is not sufficient; one rather has to find a way of visualizing the response of

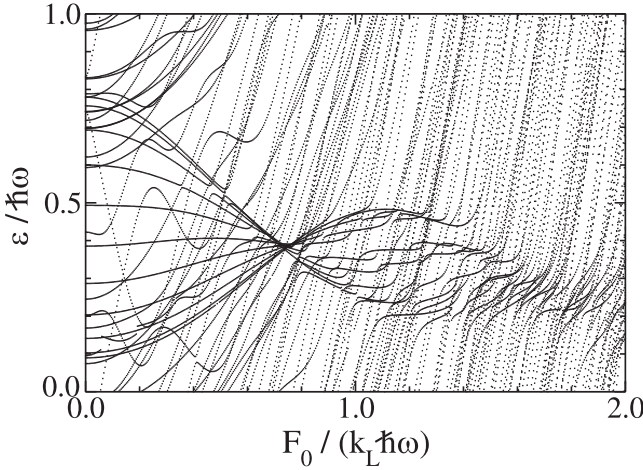


**Figure 7.** Quasienergy band originating from the lowest energy band for  $V_0/E_R = 4.0$  and  $\hbar\omega/E_R = 0.5$ , embedded in a host of quasienergies from other bands. Shown are quasienergy eigenvalues with reduced wave numbers  $k/k_L$  varying between 0.0 and 1.0 in steps of 0.1. To produce this figure, the Floquet states have been ordered according to their overlap with the basis states, and only quasienergies belonging to the respective three ‘lowest’ Floquet states have been plotted. In the coarse-graining regime where the band is still recognizable as such, Floquet wave packets (106) are protected against heating, whereas the system would heat up soon in the resonance-dominated regime.

entire quasienergy bands to the drive. To this end, we have combined in figure 7 quasienergies with 11 reduced wave numbers  $k/k_L = 0.0, 0.1, \dots, 1.0$ , for the same parameters as employed in figure 6. After each solution of the eigenvalue equation for the respective prescribed values of  $k/k_L$  and  $\beta$  the Floquet states have been ordered according to their overlap with the basis states as discussed for the particle in the box in section 3.3, and only the quasienergies of the respective three ‘lowest’ Floquet states have been included in the plot. Because of the multitude of avoided crossings involved, this procedure cannot always give smooth lines, but it clearly brings out the key features: The *internal* ac-Stark shift, that is, the ac-Stark shift of states with different  $k/k_L$  within the same band relative to each other, effectuates a narrowing of the quasienergy band emerging from the lowest energy band  $n = 0$  when  $\beta$  is increased from zero, such that the width of this quasienergy band approaches zero when  $\beta \approx 0.74$ . The width increases again when  $\beta$  is enlarged still further, but for  $\beta > 1.0$  the band is virtually torn apart by a plethora of multiphoton resonances with ac-Stark-shifted other bands. This figure 7 also exemplifies what the concept of coarse graining, as introduced in section 3.5, means in practice: in the coarse-graining regime, where the quasienergy band remains almost intact, a Floquet wave packet (106) prepared in this band hardly couples to higher ones, so that the system is well protected against heating, whereas it would be subject to rapid heating in the resonance-dominated regime.

Since the gap  $\Delta_{01}$  here amounts to the energy of about four ‘photons’, the driven lowest energy band remains reasonably well isolated from the higher ones at least for low

driving amplitudes. In this case one can resort to a single-band approximation: provided the lattice is so deep that the lowest Wannier state localized in one of the lattice wells has appreciable overlap with its nearest neighbors only [77], the unperturbed lowest energy band acquires a cosine form,

$$E_0(k) = E_c - \frac{W_0}{2} \cos(ka), \quad (131)$$

where  $a$  is the lattice constant. In the case of optical cosine lattices the relative error of this approximation still is on the order of 7% when  $V_0/E_R = 4.0$ , and drops to 2% when  $V_0/E_R = 8.0$  [10, 78]. When an isolated cosine band (131) is driven by a sinusoidal force (121) the calculation of the resulting quasienergy band becomes elementary, giving [10, 69, 79]

$$\varepsilon_0(k) = E_c - \frac{W_0}{2} J_0\left(\frac{F_0 a}{\hbar\omega}\right) \cos(ka) \bmod \hbar\omega. \quad (132)$$

Here  $J_0(z)$  is the Bessel function of order zero. Starting from  $J_0(0) = 1$  this function oscillates with increasing real argument  $z$ , with an amplitude decreasing as  $1/\sqrt{z}$ ; its first two zeros are located at  $z_1 \approx 2.405$  and  $z_2 \approx 5.520$  [80]. Thus, the result (132) derived for a perfectly isolated band explains part of the observations made in figure 7. At the zeros of the Bessel function the width of the band (132) vanishes, so that it becomes dispersionless. Since  $a = \pi/k_L$  for optical cosine lattices, we have

$$\frac{F_0 a}{\hbar\omega} = \pi\beta, \quad (133)$$

implying that the first band flattening can occur when the scaled driving amplitude (130) adopts the value

$$\beta_1 = z_1/\pi \approx 0.765; \quad (134)$$

the second ‘collapse point’ is located at

$$\beta_2 = z_2/\pi \approx 1.757 \quad (135)$$

in the ideal case.

In contrast to the assumptions underlying the single-band expression (132), a driven energy band in an optical lattice is not isolated, but subject to interband transitions. Hence, the quasienergy band emerging from the lowest energy band incorporates these transitions by acquiring admixtures from higher energy bands. Even if the energy gap  $\Delta_{01}$  amounts to the energy of several ‘photons’, so that, perturbatively speaking, it can only be bridged by higher-order multiphoton transitions, this hybridization is nonnegligible when the scaled driving amplitude  $\beta$  becomes nonperturbatively strong. This is precisely what is seen in figure 7: for  $\beta < 1$  multiphoton resonances still play a minor role, so that equation (132) describes the exact numerical data reasonably well in this interval, in the ‘coarse graining’ sense put forward in section 3.5. In particular, an approximate band collapse is observed at  $\beta \approx 0.74$ , quite close to the predicted value (134). But for  $\beta > 1.5$  the resonances become so strong that the band is almost completely disrupted, so that coarse graining becomes impossible and a second band collapse cannot be realized. The increasing importance of multiphoton resonances with increasing  $\beta$  becomes particularly evident in

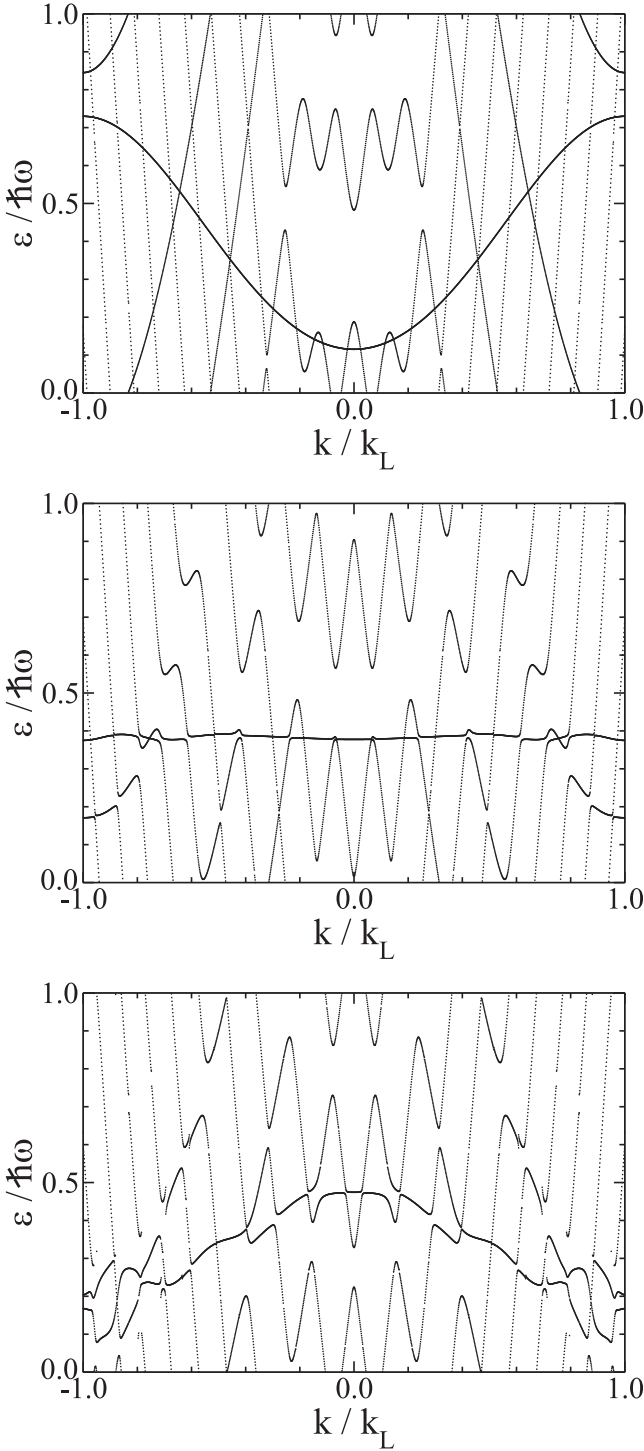


**Figure 8.** Quasienergy dispersion relations for  $V_0/E_R = 4.0$  and  $\hbar\omega/E_R = 0.5$ , implying that the gap  $\Delta_{01}$  between the lowest and the first excited unperturbed energy band is a bit smaller than  $4\hbar\omega$  (see table 1). For scaled driving amplitude  $\beta = 0.20$  the quasienergy band originating from the lowest energy band still is well described by the single-band approximation (132) (upper panel). For  $\beta = 0.74$ , corresponding to the ‘collapse point’ observed in figure 7, the band is not perfectly flat, but rather disrupted by several small anticrossings (middle panel). For  $\beta = 1.21$ , for which an isolated band (132) would be maximally inverted, strong hybridization occurs (lower panel), forecasting rapid heating.

figure 8, where we have visualized the quasienergy dispersion relation of the quasienergy band emerging from the ground-state energy band; again these plots have been produced by selecting the ‘lowest’ three quasienergies for each value of the reduced wave number  $k/k_L$ . In the upper panel of figure 8 we have  $\beta = 0.2$ ; here the cosine band (132) is well preserved. It should be kept in mind, however, that the coarse graining philosophy is implied already here: lots of (in fact, infinitely many) nonresolved anticrossings are tacitly swept under the carpet. In the middle panel we have  $\beta = 0.74$ , corresponding to the smallest band width found in figure 7. Evidently the quasienergy band is ‘essentially’ flat, but it is already visibly affected by quite a number of narrow resonances. When  $\beta = 1.21$  the ideal band (132) would be maximally inverted, because the Bessel function takes on its largest negative value here. But, as seen in the lower panel of figure 8, the actual quasienergy band then hybridizes strongly, developing wide anticrossings which render a single-band description useless. In experimental terms, the widths of these anticrossings quantify the strength of the coupling of the system’s wave function to higher states, assuming that it had initially been prepared in the lowest band, and thus determine the time scales associated with heating: while a weakly interacting Bose gas in a driven optical lattice remains shielded against heating in the coarse-graining regime for hundreds or thousands of driving cycles [7, 10], it would heat up much faster, and be lost from the lattice, when the resonances start to make themselves felt.

Hence, one of the appealing prospects offered by driven optical lattices is that one can easily reach the realm of nonperturbatively strong driving, which would not be accessible in an equally clean manner with laser-driven electrons in crystal lattice potentials, say. The scaled driving amplitude (130) is related to the shaking amplitude  $\Delta L$  entering into the laboratory-frame Hamiltonian (112) through

$$\beta = \frac{\pi}{2} \frac{\hbar\omega}{E_R} \frac{\Delta L}{a}, \quad (136)$$

so that values of  $\beta$  on the order of unity can be reached when  $\Delta L$  is comparable to the lattice constant  $a$ . In this sense, driven optical lattices filled with ultracold atoms may serve as ‘strong field simulators’, allowing one to probe multiphoton transitions in a periodic potential without encountering the many competing charge-induced effects that would mask them in solid-state samples interacting with laser fields of equivalent strengths [81, 82].

#### 4.4. Isolating a single cosine quasienergy band

If, however, one desires to come closer to the single-band ideal (132) than in the previous example, and to engineer practically flat or perfectly inverted cosine bands, the ‘degree of isolation’ of the ground-state energy band has to be enhanced. This can be achieved, for instance, by increasing the lattice depth, which amounts to an enlargement of the gap  $\Delta_{01}$ , while keeping the driving frequency at its previous

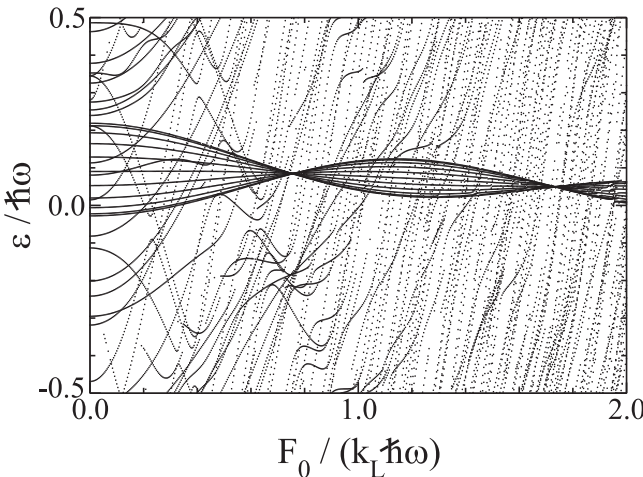


**Figure 9.** Quasienergy band for  $V_0/E_R = 8.0$  and  $\hbar\omega/E_R = 0.5$ , so that  $\Delta_{01} = 7.54 \hbar\omega$  here. This plot has been produced in the same manner as figure 7.

value. Following that strategy, figure 9 depicts the ‘lowest’ quasienergy band for  $V_0/E_R = 8.0$  and  $\hbar\omega/E_R = 0.5$ . According to table 1 this implies  $\Delta_{01}/(\hbar\omega) = 7.54$ , so that now more than seven ‘photons’ are required to bridge the gap, whereas it had been about four in figure 7. Consequently one now obtains a quasienergy band which remains more or less intact even up to  $\beta = 2.0$ , with two collapse points at the predicted positions (134) and (135). The validity of equation (132) is confirmed in greater detail by figure 10: the cosine band starts to narrow when  $\beta = 0.2$  (upper panel), becomes perfectly flat—at least on the scale of figure 10; coarse graining still is implied here!—when  $\beta = 0.76$  (middle panel), and is maximally inverted when  $\beta = 1.21$  (lower panel). It is interesting to observe how the attempted flattening of a second band at  $\beta = 0.76$  is thwarted by an aligned sequence of broad resonances.

The feasibility of close-to-perfect band inversion in real optical lattices has a noteworthy consequence: A weakly interacting Bose–Einstein condensate occupies the state with  $k/k_L = \pm 1$  when the band is inverted [83], instead of the usual ground state  $k/k_L = 0$  of an undriven cosine band (131). It also deserves to be mentioned that first indications for band narrowing in periodically driven optical lattices loaded with cold, but noncondensed atoms had been observed in pioneering experiments as early as 1998 [84], but the Bessel function could not be mapped out cleanly beyond the first collapse point until a decade later through experiments with driven Bose–Einstein condensates [7, 10].

Thus, for carefully selected parameters the quasienergy band which emerges in a sinusoidally driven optical lattice from its lowest energy band is well described by equation (132). This observation creates a link to the subject of dynamic localization: it had been theoretically discussed already in 1986 that a charged particle moving under the influence of an oscillating electric field on a defect-free single-band tight-binding lattice with equal couplings between neighboring sites remains ‘dynamically’ localized when the

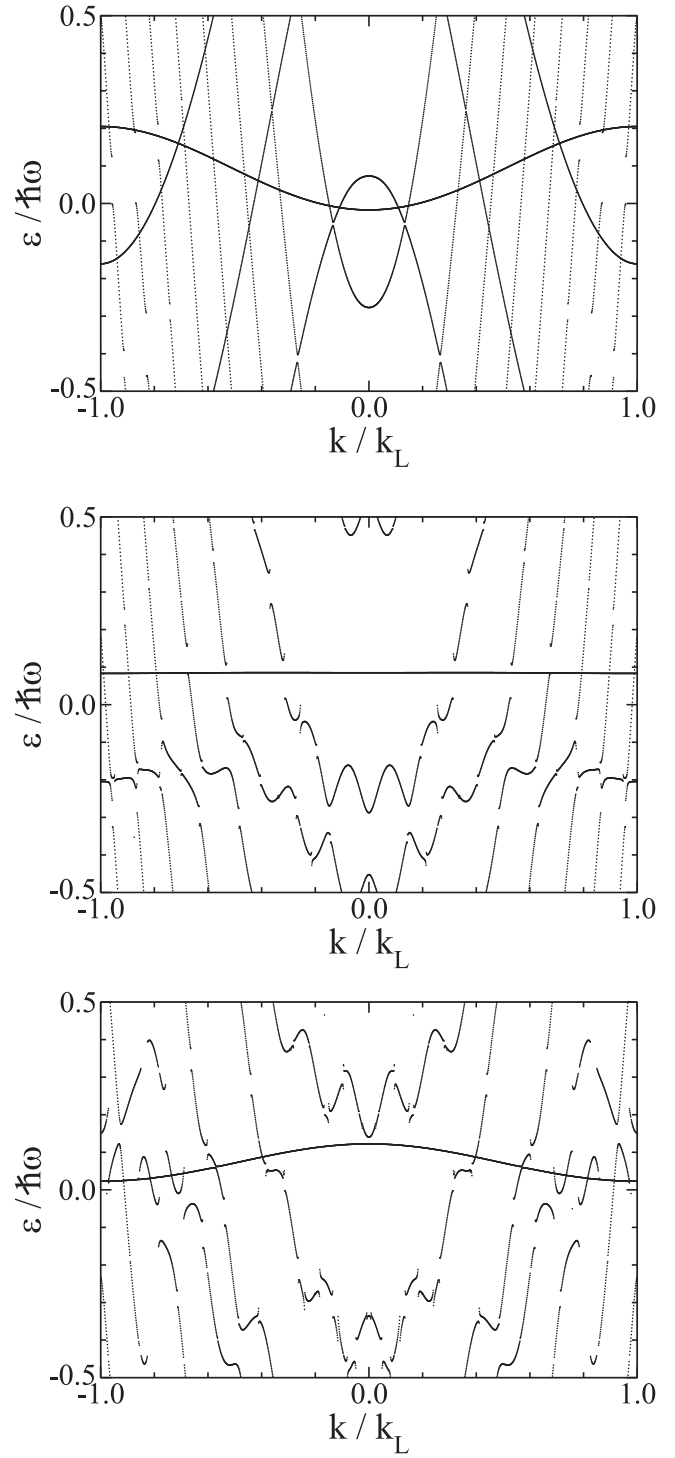


**Figure 10.** Quasienergy dispersion relations for  $V_0/E_R = 8.0$  and  $\hbar\omega/E_R = 0.5$ . For  $\beta = 0.2$  (upper panel),  $\beta = 0.76$  (middle panel), and  $\beta = 1.21$  (lower panel) the coarse-grained quasienergy band emerging from the lowest energy band is well described by the single-band formula (132).

parameter  $F_0 a/(\hbar\omega)$  equals a zero of the Bessel function  $J_0$ , with  $F_0$  denoting the product of the particle’s charge and the amplitude of the electric field [85]. The introduction of quasienergy bands [69, 79] allows one to understand this remarkable phenomenon within the established concepts of solid-state physics: if one builds an arbitrary wave

packet (106) from the spatio-temporal Bloch waves which form a quasienergy band (132) and follows its evolution in time, the components of this packet generally will dephase, so that the packet generally will delocalize, except for those parameters for which the band is dispersionless, i.e., when  $F_0 a / (\hbar\omega)$  equals a zero of  $J_0$ . Then all Floquet components of the wave packet acquire precisely the same phase factor after each driving cycle, so that the packet reproduces itself perpetually. Hence, dynamic localization results from prohibited dephasing [86].

Since the width of an ideal cosine band is determined by the hopping matrix elements between neighboring sites, the appearance of the Bessel function  $J_0$  in the quasienergy band (132) may be interpreted as an effective renormalization of these hopping matrix elements caused by the oscillating force. This view leads to a number of further applications. For instance, a tight-binding chain with quasiperiodically varying on-site energies exhibits a metal-insulator transition at a certain critical ratio of the quasiperiodic perturbation strength and the hopping strength [87, 88]. Since the driving-induced renormalization of the hopping strength allows one to tune this ratio by applying an oscillating force, one encounters a new mechanism for switching from one phase to the other: the magnitude of the driving amplitude decides whether the system is in the ‘metallic’ or in the ‘insulating’ phase; this engineering option can be explored with ultracold atoms in driven bichromatic optical lattices [70, 86, 89]. By the same token, the average extension of Anderson-localized states in a randomly perturbed lattice is determined by the ratio of the typical strength of the random on-site perturbation and the hopping strength; accordingly, the degree of Anderson localization can be controlled by an external oscillating force [90]. Of particular significance is the recognition that the concept of hopping-strength renormalization survives the presence of interparticle interaction in many-body systems [91, 92]. Namely, the prototypal quantum phase transition from a superfluid to a Mott insulator undergone by a gas of ultracold atoms in an optical lattice [93] is governed by the ratio of the on-site interaction strength and the nearest-neighbor hopping strength. Therefore, the phase boundary can be crossed in a periodically driven optical lattice by varying the driving amplitude [91], as has been confirmed precisely in a path-directing experiment by Zenesini *et al* [11]. In line with this proof of principle, related theoretical proposals for controlling the phase transition have been made [92, 94], and the driving-induced renormalization of the hopping strength has been exploited still further in a recent series of quite different innovative optical-lattice experiments [14, 17, 19–21, 23]. A concise discussion of the current status of these topical developments is given by Eckardt [26].

#### 4.5. Floquet engineering with interband ac-Stark shifts

Flat-band engineering and band inversion, as exemplified in figure 10, rely on the internal ac-Stark effect within a single band. The exploitation of the *interband* ac-Stark effect, that is, of the driving-induced shift of different bands relative to each other, opens up further options. A seminal example of this

type of Floquet engineering has been provided by Parker *et al* [22]: after loading a Bose–Einstein condensate of  $^{133}\text{Cs}$  atoms into an optical lattice created with laser wavelength  $\lambda = 1064$  nm, amounting to the recoil frequency  $E_R/h = 1.325$  kHz, these authors have coupled the lowest two energy bands by employing a driving frequency which is blue-detuned from a transition between them: working with a lattice of depth  $V_0/E_R = 7.0$ , one finds the scaled band separation  $E_1(0) - E_0(0) = 4.96 E_R$  at  $k/k_L = 0$ , while  $E_1(\pm 1) - E_0(\pm 1) = 3.34 E_R$  at  $k/k_L = \pm 1$ ; shaking that lattice with frequency  $\omega/(2\pi) = 7.3$  kHz, or  $\hbar\omega/E_R = 5.51$ , then gives a blue-detuning by about 11% at  $k/k_L = 0$ , but by about 65% at  $k/k_L = \pm 1$  [22].

As shown in the upper panel of figure 11, for low driving amplitudes this choice of parameters places the lowest band  $n = 0$  half-way between the first excited band  $n = 1$  and the second excited band  $n = 2$  in the quasienergy Brillouin zone. For moderate driving strength one may then regard the coupled lowest two bands  $n = 0$  and  $n = 1$  as set of two-level systems, parametrized by the wave number  $k/k_L$ ; each one behaving in accordance with the RWA-formula (65). Recalling the assignment (62) for blue detuning, the quasienergy representatives connected to the ground-state band  $n = 0$  then are shifted upwards with increasing driving amplitude, whereas the representatives connected to the excited band  $n = 1$  are shifted downwards. Now the detuning varies throughout the quasimomentum Brillouin zone, being smallest at its center  $k/k_L = 0$  and being largest at the edges  $k/k_L = \pm 1$ . According to the expression (58) for the generalized Rabi frequency, this implies that the upwards-ac-Stark shift of the lowest band is largest at the zone center, and smallest at the edges; in combination with the already existing curvature of the unperturbed energy band these unequal shifts result in the formation of a double well-shaped quasienergy dispersion relation. This mechanism is illustrated in figure 12 for the parameters employed in the experiment [22]; with the help of the relation (136) the scaled driving strengths  $\beta = 0.17, 0.35, 0.52$ , and  $0.69$  are converted into the peak-to-peak shaking amplitudes  $\Delta x = 2 \Delta L = 21$  nm, 43 nm, 64 nm, and 85 nm, respectively.

This double well-shaped quasienergy dispersion is of profound experimental significance, since a driven Bose gas condenses into one of the two wells, allowing one to simulate ferromagnetism [22]; if interparticle interactions are taken into account by means of a Bogoliubov treatment, one obtains a ‘roton-maxon’ dispersion as known from He II [24]. So far one works with relatively low shaking amplitudes, avoiding the resonances which show up strongly in figure 12 in the center of the barrier for  $\beta = 0.69$ ; the expanded view provided by the middle panel of figure 11 allows one to trace the anticrossing partner to the ‘above barrier’-band  $n = 3$ . However, for substantially higher driving amplitudes such as  $\beta = 1.5$  considered in the lower panel of figure 11, the quasienergy bands have disentangled themselves, creating a quite pronounced, smooth double-well structure in the center of the quasimomentum Brillouin zone. Thus, if one succeeds in populating the corresponding quasienergy band, the strongly driven system may actually be more stable than one with

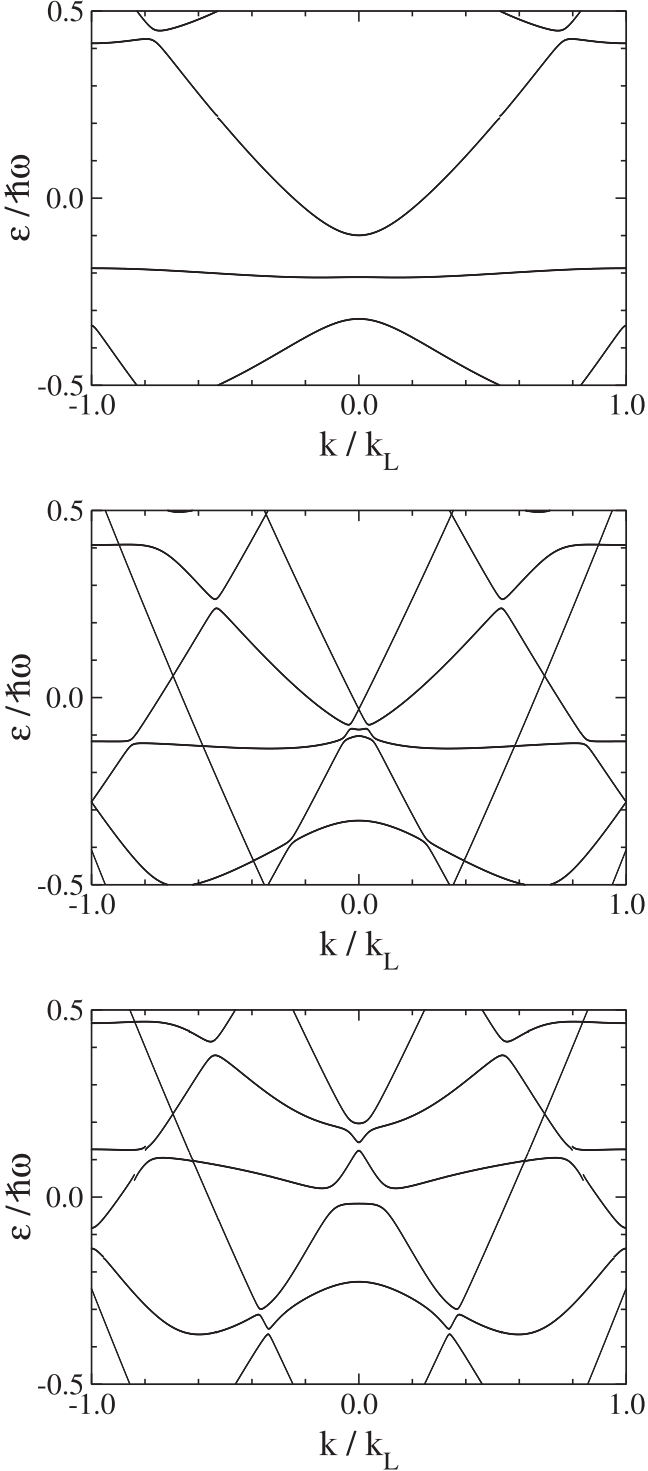


**Figure 11.** Quasienergy dispersion relations for  $V_0/E_R = 7.0$  and  $\hbar\omega/E_R = 5.51$ , as corresponding to [22]. For  $\beta = 0.17$  (upper panel) the ‘lowest’ quasienergy band  $n = 0$ , pinched between the bands  $n = 1$  (below) and  $n = 2$  (above) in the quasienergy Brillouin zone, exhibits a shallow double-well structure, as magnified in figure 12. For  $\beta = 0.69$  (middle panel) the ac-Stark-shifted ground-state band resonates with driven free particle-like above-barrier states. For  $\beta = 1.50$  (lower panel) the avoided crossings have become wider, leading to an even more pronounced double-well structure close to the center of the quasimomentum Brillouin zone.

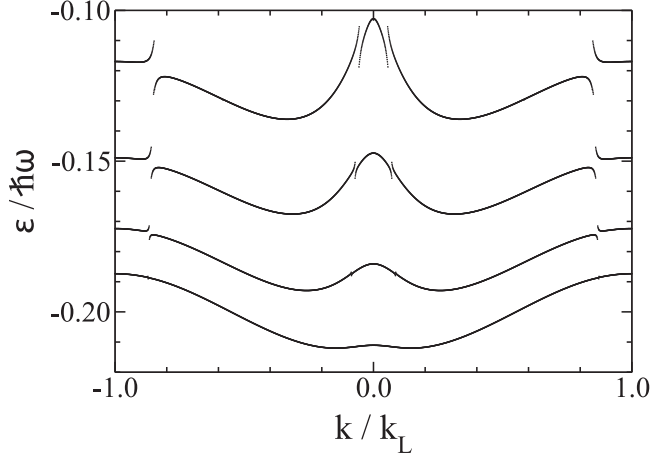


**Figure 12.** Ac-Stark-shifted quasienergy band emerging from the ground-state energy band of an optical lattice with depth  $V_0/E_R = 7.0$  under driving with frequency  $\hbar\omega/E_R = 5.51$ . The driving amplitudes  $\beta$  are 0.17, 0.35, 0.52, and 0.69 (bottom to top). The avoided crossings result from multiphoton resonances with the band  $n = 3$ , providing a potential escape channel. This figure corresponds precisely to figure S2 shown in the supplementary information of [22].

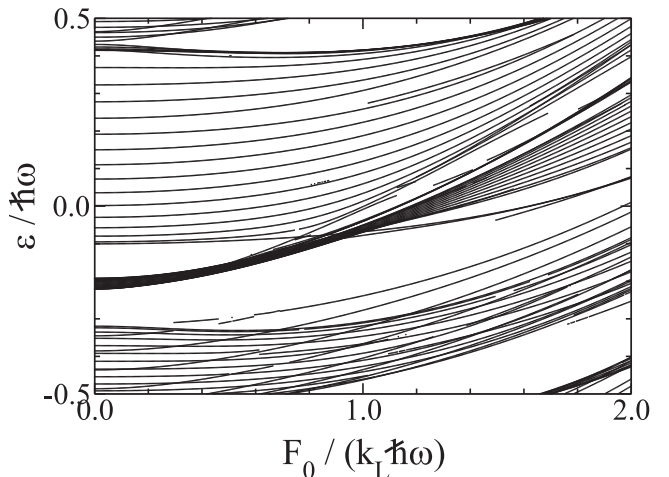


**Figure 13.** Lowest three quasienergy bands for  $V_0/E_R = 7.0$  and  $\hbar\omega/E_R = 5.51$  (see figure 11); each band is represented by 21 scaled wave numbers  $k/k_L$  ranging from 0 to 1 in equal steps of 0.05. Observe how the quasienergy band  $n = 0$  widens after touching its upper partner  $n = 2$ , whereas that latter band becomes more narrow, indicating strong ‘vertical’ hybridization of both bands.

lower driving amplitudes, but one has to find a way to protect the atoms from the intermediate resonances encountered when the drive is turned on.

Another peculiar strong-driving phenomenon is depicted in figure 13: similar to figures 7 and 9, here we have plotted the quasienergies emanating from the three lowest energy bands versus the scaled driving amplitude, now for 21 wave numbers  $k/k_L$  ranging from 0 to 1 in steps of 0.05. Interestingly, the bands  $n = 0$  and  $n = 2$  touch at  $\beta \approx 0.8$ , and then hybridize strongly: the quasienergy band  $n = 0$  fans out and widens, whereas its partner  $n = 2$  becomes more narrow.

This type of resonant band hybridization is the subject of the following section.

#### 4.6. Floquet engineering with resonances

In the previous example multiphoton resonances have been considered to be detrimental, causing unwanted transitions that should be avoided. But such resonances also constitute one of the most powerful tools of Floquet engineering: resonances not only shift quasienergy curves, but they also break them up and create new connections. Seen from a conceptual viewpoint, usual energy bands result from (energetically) ‘horizontal’ hybridization, that is, by forming Bloch bands from energetically aligned Wannier states localized at the different lattice sites [77]. In contrast, quasienergy band formation can also involve ‘vertical’ hybridization when different Wannier states localized at the *same* site are efficiently coupled by the oscillating force, as is achieved by choosing a matching frequency. This option, which has no counterpart in standard solid-state physics, can be exploited to design dispersion relations not found with any time-independent lattice. To illustrate this decisive feature, we again consider lattices with depth  $V_0/E_R = 7.0$ , as in figure 11, but now with the lower driving frequency  $\hbar\omega/E_R = 4.15$ , which equals the separation of the lowest two energy bands at  $k/k_L \approx \pm 0.41$ . As seen in the upper panel of figure 14, this single-photon resonance causes a relatively wide anticrossing of the bands  $n = 0$  and  $n = 1$  even for a driving amplitude as small as  $\beta = 0.1$ , while the bands  $n = 1$  and  $n = 2$  undergo an anticrossing at  $k/k_L \approx \pm 0.55$ . With increasing driving strength these avoided band crossings become wider, leading at  $\beta = 0.5$  (middle panel) to a double-well dispersion with minima spaced by  $\Delta k/k_L \approx 0.9$ , about twice as wide as those previously displayed in figure 12. This ability to purposefully engineer such wide double well-shaped dispersion relations may be of some experimental interest: While the condensate wave function collapses into one of the two minima when these minima are close [22, 24], this might no longer be so when they are farther apart, possibly providing information on the condensate’s coherence. But again, one has to take care of additional unwanted narrow resonances with driven free particle-like above-barrier states which inevitably will show up under strong driving: as shown in the lower panel of figure 14, two such resonances puncture the double well right at its bottom when  $\beta = 1.0$ , opening up efficient channels of escape which might not be desirable.

But there is still more. If one inspects the development of the quasienergy bands with increasing driving amplitude under these resonant conditions, as displayed in figure 15, one finds that the assignment of band indices in the strong-driving regime is anything but obvious; as a result of the resonant piercing of one band by another, additional bands seem to appear. Such a reorganization of the band structure with increasing driving strength necessarily gives rise to highly unusual dynamics of Floquet wave packets (106) populating an individual quasienergy band. The possibility to systematically engineer, experiment with, and utilize such exotic band structures may well constitute one of the greatest new chances offered by periodically driven optical lattices.

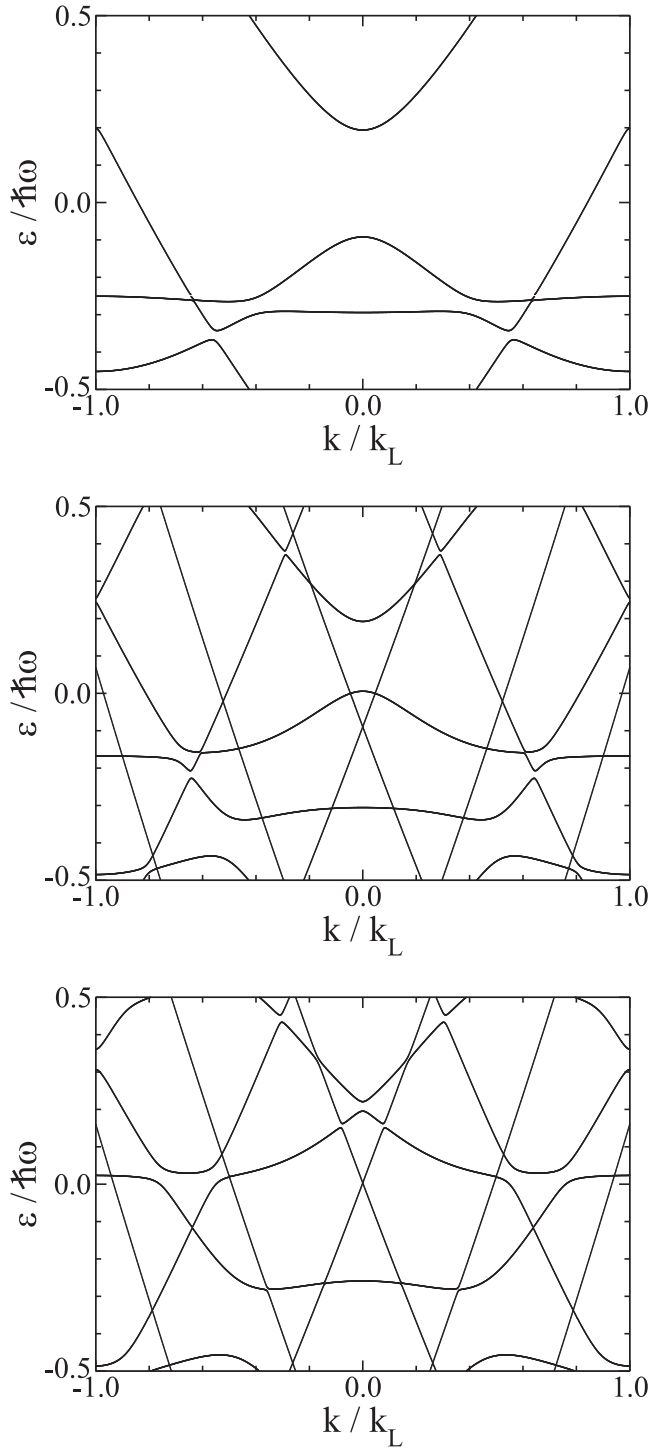


**Figure 14.** Quasienergy dispersion relations for  $V_0/E_R = 7.0$  and  $\hbar\omega/E_R = 4.15$ , providing a single-photon resonance between the lowest two energy bands. Scaled driving amplitudes are  $\beta = 0.1$  (upper panel),  $\beta = 0.5$  (middle panel), and  $\beta = 1.0$  (lower panel). Observe how the wide double-well dispersion created with  $\beta = 0.5$  from the ground-state band is punctured by narrow resonances when  $\beta = 1.0$ .

## 5. Conclusions and outlook

The preceding study has led to some computational insights which deserve to be formulated here, and to some more

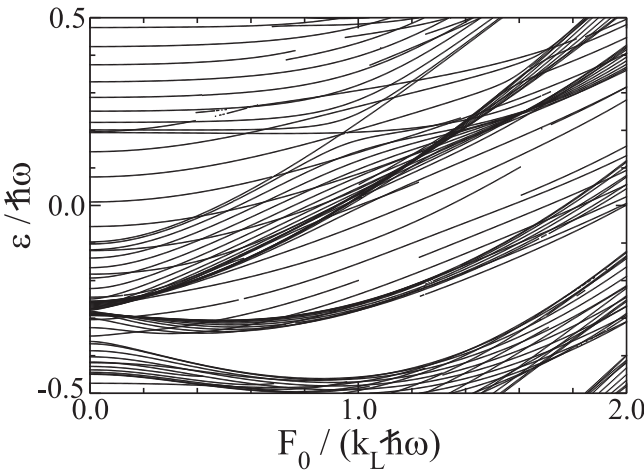


**Figure 15.** Quasienergy bands for  $V_0/E_R = 7.0$  and  $\hbar\omega/E_R = 4.15$  (see figure 14). As in figure 13, only quasienergy representatives emanating from the lowest three energy bands are plotted; each such band is represented by 21 equally spaced scaled wave numbers  $k/k_L$ . Observe that there appear to be more than three quasienergy bands in the strong-driving regime.

general conceptual issues which may inspire future experiments.

To begin with, the quasienergy eigenvalue problem for a driven optical lattice is quite similar to that for the driven particle in a box discussed in section 3.3, except that the wave number  $k$  appears as an additional parameter for given values of the driving frequency and driving amplitude. Since the external force, when built into the optical-lattice Hamiltonian in one of the equivalent forms (89), (94), or (112), does not couple unperturbed Bloch waves with different wave numbers, and since the energy of Bloch states with the same wave number grows about quadratically with the band index, efficient coupling occurs only between a limited number of states, greatly facilitating the numerical task for any fixed wave number. But still, one has to keep track of all wave numbers within one quasimomentum Brillouin zone to map out the band structure. Therefore, the resulting quasienergy bands may give rise to fairly complicated dynamics, as exemplified by figure 7. Here the concept of coarse graining comes into play: if one may safely neglect all ‘small’ quasienergy anticrossings, it may be possible to describe the driven system by an effective time-independent Hamiltonian within the subspace considered [25]. The viability of this concept is illustrated by figure 9: while it is still not possible to construct the full time-independent operator  $G$  which governs the driven optical lattice in the sense of the transformed Schrödinger equation (52), one may restrict oneself to the dynamics within the lowest undriven energy band under the conditions of figure 9, and describe these dynamics in terms of an effective time-independent Hamiltonian possessing only one single cosine energy band (132), ignoring the mod  $\hbar\omega$ -indeterminacy of the original quasienergies. Whether or not such a coarse graining approach is feasible also depends on the time scale of the experiment. A small anticrossing of width  $\delta\epsilon$  may reasonably be ignored on time scales which are short compared to  $\hbar/\delta\epsilon$ , but will make itself felt on

longer time scales. Thus, it should be of interest to perform detailed measurements of the times required for heating, or simply for loss of particles from a driven optical lattice. Expressed differently, systematic measurement of heating rates of ultracold atoms in driven optical lattices constitutes a means of quasienergy band spectroscopy.

The experimental exploration of the close connection between avoided crossings of quasienergies and multiphoton resonances would be most illuminating in situations in which only relatively few, large anticrossings dominate the dynamics. Such situations can be deliberately engineered by vertical hybridization, in the sense explained when discussing figure 14. The future study of such multiphoton resonances with Bose–Einstein condensates in driven optical lattices would allow one to systematically address the influence of interparticle interactions on multiphoton transitions, with a clarity which probably will remain unachievable in experiments with crystalline solids exposed to laser radiation, thus creating an altogether new crosslink between the dynamics in strong laser fields and the physics of ultracold atoms. The recently reported, groundbreaking first experimental results obtained along these lines [95] suggest that this optimistic view may not be unjustified.

Such optical-lattice experiments aiming to utilize multiphoton-like transitions with ultracold atoms will gain additional handles of control if they are not performed simply with long ac driving, but rather with short pulses possessing a smooth envelope. In such cases the quasienergy bands  $\epsilon_n(k)$ , considered for all instantaneous driving strengths, form ‘quasienergy surfaces’ on which the system’s wave function can evolve in an effectively adiabatic manner as long as it does not encounter large avoided crossings, whereas it undergoes Landau–Zener-like transitions at such anticrossings, similar to the pulsed particle in a box examined in figure 4. But with pulsed optical lattices such anticrossings would couple quasienergy surfaces only in the vicinity of certain wave numbers, as illustrated by figure 14. Therefore, one could exploit such anticrossings with driven optical lattices for selectively manipulating only certain components of given wave packets, leaving others unaffected [96]. Such pulse experiments could be given a further level of sophistication if they were combined with the feedback-techniques of optimal control, as they are used in chemical physics in order to design specific laser pulses for the coherent control of molecular dynamics [97–99]. In this manner, one could iteratively adapt the pulses’ properties such that they result, for instance, in the preparation of particularly interesting target states which may not be accessible by more conventional means: Instead of ‘teaching lasers to control molecules’ [97], one then teaches optical lattices to control Bose–Einstein condensates.

Ultracold atoms in optical lattices so far have created an immensely fruitful link between experimental atomic physics and the physics of condensed-matter systems [1–3]. It stands to reason that the further investigation of ultracold atoms in time-dependent optical lattices, driven either periodically or by pulses, will add a new dimension to this field.

## Acknowledgments

I would like to express my gratitude to all colleagues and collaborators who have taught me many of the subjects collected here, with particular thanks to Heinz-Peter Breuer, Klaus Dreser, André Eckardt, and Stephan Arlinghaus. This work was supported by the Deutsche Forschungsgemeinschaft (DFG) through grant no. HO 1771/6-2.

## Appendix. Use of symmetries

The most time-consuming step in the numerical computation of Floquet states and their quasienergies is the determination of the monodromy matrix. By exploiting the symmetries of the quasienergy operator for a sinusoidally driven optical cosine lattice, the numerical effort is reduced by a factor of two.

Let  $\tilde{H}(z, \tau)$  denote the scaled Hamiltonian appearing on the right-hand side of equation (129), multiplied by  $E_R/(\hbar\omega)$ , so that the scaled quasienergy eigenvalue equation for the driven lattice takes the form

$$\left( \tilde{H}(z, \tau) - i \frac{d}{d\tau} \right) u(z, \tau) = \frac{\varepsilon}{\hbar\omega} u(z, \tau), \quad (\text{A1})$$

with one period of the dimensionless time  $\tau$  having the length  $2\pi$ . The quasienergy operator here remains invariant under the combined operation

$$\tilde{P} : \begin{cases} z \rightarrow -z \\ \tau \rightarrow \pi - \tau \\ \text{complex conjugation} \end{cases} \quad (\text{A2})$$

which implies

$$u(z, \tau) = u^*(-z, \pi - \tau) \quad (\text{A3})$$

for each Floquet eigenfunction. In particular, this gives the identities

$$\begin{aligned} u(z, \pi/2) &= u^*(-z, \pi/2) \\ u(z, 0) &= u^*(-z, \pi). \end{aligned} \quad (\text{A4})$$

Now the time-evolution operator for the first quarter cycle, ranging from 0 to  $\pi/2$ , is written as

$$\tilde{U}(\pi/2, 0) = \sum_n u_n(z, \pi/2) u_n^*(z', 0) e^{-i\alpha_n}, \quad (\text{A5})$$

where

$$\alpha_n = \frac{\varepsilon_n \pi}{\hbar\omega} = \frac{\varepsilon_n T/4}{\hbar} \quad (\text{A6})$$

abbreviate the accompanying phases. Using the notation

$$\varphi_\mu(z) = \langle z | \mu \rangle \quad (\text{A7})$$

for the trigonometric basis functions (20) and (21), one thus has the matrix elements

$$\tilde{U}(\pi/2, 0)_{\mu\nu} = \sum_n \langle \mu | u_n(\pi/2) \rangle \langle u_n(0) | \nu \rangle e^{-i\alpha_n}. \quad (\text{A8})$$

Next, the evolution operator for the second quarter cycle reads

$$\begin{aligned} \tilde{U}(\pi, \pi/2) &= \sum_n u_n(z, \pi) u_n^*(z', \pi/2) e^{-i\alpha_n} \\ &= \sum_n u_n^*(-z, 0) u_n(-z', \pi/2) e^{-i\alpha_n}, \end{aligned} \quad (\text{A9})$$

where the symmetries (A4) have been used. Observing now that the basis functions (A7) have (ordinary) parity  $(-1)^\mu$ , this gives

$$\begin{aligned} \tilde{U}(\pi, \pi/2)_{\mu\nu} &= (-1)^{\mu+\nu} \sum_n \langle u_n(0) | \mu \rangle \langle \nu | u_n(\pi/2) \rangle e^{-i\alpha_n} \\ &= (-1)^{\mu+\nu} \tilde{U}(\pi/2, 0)_{\nu\mu}. \end{aligned} \quad (\text{A10})$$

Thus, having computed the evolution matrix for the first quarter cycle one deduces its continuation for the second quarter cycle by symmetry; a corresponding identity connects  $\tilde{U}(2\pi, 3\pi/2)$  and  $\tilde{U}(3\pi/2, \pi)$ .

## References

- [1] Morsch O and Oberthaler M 2006 Dynamics of Bose-Einstein condensates in optical lattices *Rev. Mod. Phys.* **78** 179
- [2] Bloch I, Dalibard J and Zwerger W 2008 Many-body physics with ultracold gases *Rev. Mod. Phys.* **80** 885
- [3] Lewenstein M, Sanpera A and Ahufinger V 2012 *Ultracold Atoms in Optical Lattices* (Oxford: Oxford University Press)
- [4] Steck D A, Oskay W H and Raizen M G 2001 Observation of chaos-assisted tunneling between islands of stability *Science* **293** 274
- [5] Hensinger W K *et al* 2001 Dynamical tunneling of ultracold atoms *Nature* **412** 52
- [6] Gemelke N, Sarajlic E, Bidel Y, Hong S and Chu S 2005 Parametric amplification of matter waves in periodically translated optical lattices *Phys. Rev. Lett.* **95** 170404
- [7] Lignier H, Sias C, Ciampini D, Singh Y, Zenesini A, Morsch O and Arimondo E 2007 Dynamical control of matter-wave tunneling in periodic potentials *Phys. Rev. Lett.* **99** 220403
- [8] Ivanov V V, Alberti A, Schioppo M, Ferrari G, Artoni M, Chiofalo M L and Tino G M 2008 Coherent delocalization of atomic wave packets in driven lattice potentials *Phys. Rev. Lett.* **100** 043602
- [9] Sias C, Lignier H, Singh Y P, Zenesini A, Ciampini D, Morsch O and Arimondo E 2008 Observation of photon-assisted tunneling in optical lattices *Phys. Rev. Lett.* **100** 040404
- [10] Eckardt A, Holthaus M, Lignier H, Zenesini A, Ciampini D, Morsch O and Arimondo E 2009 Exploring dynamic localization with a Bose-Einstein condensate *Phys. Rev. A* **79** 013611
- [11] Zenesini A, Lignier H, Ciampini D, Morsch O and Arimondo E 2009 Coherent control of dressed matter waves *Phys. Rev. Lett.* **102** 100403
- [12] Alberti A, Ivanov V V, Tino G M and Ferrari G 2009 Engineering the quantum transport of atomic wavefunctions over macroscopic distances *Nat. Phys.* **5** 547
- [13] Haller E, Hart R, Mark M J, Danzl J G, Reichsöllner L and Nägele H-C 2010 Inducing transport in a dissipation-free lattice with super-Bloch oscillations *Phys. Rev. Lett.* **104** 200403
- [14] Struck J, Ölschläger C, Le Targat R, Soltan-Panahi P, Eckardt A, Lewenstein M, Windpassinger P and Sengstock K 2011 Quantum simulation of frustrated

- classical magnetism in triangular optical lattices *Science* **333** 996
- [15] Ma R, Tai M E, Preiss P M, Bakr W S, Simon J and Greiner M 2011 Photon-assisted tunneling in a biased strongly correlated Bose gas *Phys. Rev. Lett.* **107** 095301
- [16] Chen Y-A, Nascimbène S, Aidelsburger M, Atala M, Trotzky S and Bloch I 2011 Controlling correlated tunneling and superexchange interactions with ac-driven optical lattices *Phys. Rev. Lett.* **107** 210405
- [17] Struck J, Ölschläger C, Weinberg M, Hauke P, Simonet J, Eckardt A, Lewenstein M, Sengstock K and Windpassinger P 2012 Tunable gauge potential for neutral and spinless particles in driven optical lattices *Phys. Rev. Lett.* **108** 225304
- [18] Hauke P *et al* 2012 Non-abelian gauge fields and topological insulators in shaken optical lattices *Phys. Rev. Lett.* **109** 145301
- [19] Struck J *et al* 2013 Engineering Ising-XY spin-models in a triangular lattice using tunable artificial gauge fields *Nat. Phys.* **9** 738
- [20] Aidelsburger M, Atala M, Lohse M, Barreiro J T, Paredes B and Bloch I 2013 Realization of the Hofstadter Hamiltonian with ultracold atoms in optical lattices *Phys. Rev. Lett.* **111** 185301
- [21] Miyake H, Siviloglou G A, Kennedy C J, Burton W C and Ketterle W 2013 Realizing the Harper Hamiltonian with laser-assisted tunneling in optical lattices *Phys. Rev. Lett.* **111** 185302
- [22] Parker C V, Ha L-C and Chin C 2013 Direct observation of effective ferromagnetic domains of cold atoms in a shaken optical lattice *Nat. Phys.* **9** 769
- [23] Jotzu G, Messer M, Desbuquois R, Lebrat M, Uehlinger T, Greif D and Esslinger T 2014 Experimental realisation of the topological Haldane model with ultracold fermions *Nature* **515** 237
- [24] Ha L-C, Clark L W, Parker C V, Anderson B M and Chin C 2015 Roton-maxon excitation spectrum of Bose condensates in a shaken optical lattice *Phys. Rev. Lett.* **114** 055301
- [25] Goldman N and Dalibard J 2014 Periodically driven quantum systems: effective Hamiltonians and engineered gauge fields *Phys. Rev. X* **4** 031027
- [26] Eckardt A Periodically driven lattices: From dynamic localization to artificial magnetism, in preparation
- [27] Slater J C 1952 A soluble problem in energy bands *Phys. Rev.* **87** 807
- [28] Blanch G 1970 Mathieu functions *Handbook of Mathematical Functions* ed M Abramowitz and I A Stegun (New York: Dover) ch 20
- [29] Paul W 1990 Electromagnetic traps for charged and neutral particles *Rev. Mod. Phys.* **62** 531
- [30] Bloch F 1929 Über die Quantenmechanik der Elektronen in Kristallgittern *Z. Phys.* **52** 555
- [31] Ashcroft N W and Mermin N D 1976 *Solid State Physics* (Fort Worth: Harcourt)
- [32] Harrison W A 1989 *Electronic Structure and the Properties of Solids* (New York: Dover)
- [33] Floquet G 1883 Sur les équations différentielles linéaires à coefficients périodiques *Ann. de l' École Normale Supérieure* **12** 47
- [34] Autler S H and Townes C H 1955 Stark effect in rapidly varying fields *Phys. Rev.* **100** 703
- [35] Shirley J H 1965 Solution of the Schrödinger equation with a Hamiltonian periodic in time *Phys. Rev.* **138** B979
- [36] Zel'dovich Y B 1966 *J. Exp. Theor. Phys.* **51** 1492
- Zel'dovich Y B 1967 The quasienergy of a quantum-mechanical system subjected to a periodic action *Sov. Phys.—JETP* **24** 1006
- [37] Ritus V I 1966 *J. Exp. Theor. Phys.* **51** 1544
- Ritus V I 1967 Shift and splitting of atomic energy levels by the field of an electromagnetic wave *Sov. Phys.—JETP* **24** 1041
- [38] Sambe H 1973 Steady states and quasienergies of a quantum-mechanical system in an oscillating field *Phys. Rev. A* **7** 2203
- [39] Fainshtein A G, Manakov N L and Rapoport L P 1978 Some general properties of quasi-energetic spectra of quantum systems in classical monochromatic fields *J. Phys. B: At. Mol. Phys.* **11** 2561
- [40] Grifoni M and Hänggi P 1998 Driven quantum tunneling *Phys. Rep.* **304** 229
- [41] Chu S-I and Telnov D A 2004 Beyond the Floquet theorem: generalized Floquet formalisms and quasienergy methods for atomic and molecular multiphoton processes in intense laser fields *Phys. Rep.* **390** 1
- [42] Howland J S 1992 Quantum stability *Schrödinger Operators: The Quantum Mechanical Many-Body Problem (Lecture Notes in Physics* vol 403) (Berlin: Springer) p 100
- [43] Sakurai J J 1994 *Modern Quantum Mechanics* (Reading: Addison-Wesley)
- [44] Daleckii J L and Krein M G 1974 *Stability of Solutions of Differential Equations in Banach Space (Translations of Mathematical Monographs* vol 43) (Providence, RI: American Mathematical Society)
- [45] Rabi I I, Ramsey N F and Schwinger J 1954 Use of rotating coordinates in magnetic resonance problems *Rev. Mod. Phys.* **26** 167
- [46] Allen L and Eberly J H 1988 *Optical Resonance and Two-Level Atoms* (New York: Dover)
- [47] Breuer H P and Holthaus M 1989 Adiabatic processes in the ionization of highly excited hydrogen atoms *Z. Phys. D* **11** 1
- [48] Langemeyer M and Holthaus M 2014 Energy flow in periodic thermodynamics *Phys. Rev. E* **89** 012101
- [49] Breuer H P, Dietz K and Holthaus M 1988 The role of avoided crossings in the dynamics of strong laser field-matter interactions *Z. Phys. D* **8** 349
- [50] Holthaus M and Hone D 1993 Quantum wells and superlattices in strong time dependent fields *Phys. Rev. B* **47** 6499
- [51] Breuer H P and Holthaus M 1989 Quantum phases and Landau-Zener transitions in oscillating fields *Phys. Lett. A* **140** 507
- [52] Dresz K and Holthaus M 1999 Floquet theory for short laser pulses *Eur. Phys. J. D* **5** 119
- [53] Baruch M C and Gallagher T F 1992 Ramsey interference fringes in single pulse microwave multiphoton transitions *Phys. Rev. Lett.* **68** 3515
- [54] Yoakum S, Sirklo L and Koch P M 1992 Stueckelberg oscillations in the multiphoton excitation of helium Rydberg atoms: observation with a pulse of coherent field and suppression by additive noise *Phys. Rev. Lett.* **69** 1919
- [55] Howland J S 1979 Scattering theory for Hamiltonians periodic in time *Indiana Univ. Math. J.* **28** 471
- [56] Howland J S 1989 Floquet operators with singular spectrum: I *Ann. Inst. Henri Poincaré* **49** 309
- Howland J S 1989 Floquet operators with singular spectrum: II *Ann. Inst. Henri Poincaré* **49** 325
- Howland J S 1998 Floquet operators with singular spectrum: III *Ann. Inst. Henri Poincaré* **69** 265
- [57] Howland J S 1992 Stability of quantum oscillators *J. Phys. A: Math. Gen.* **25** 5177
- [58] Joye A 1994 Absence of absolutely continuous spectrum of Floquet operators *J. Stat. Phys.* **75** 929
- [59] Breuer H P and Holthaus M 1991 A semiclassical theory of quasienergies and Floquet wave functions *Ann. Phys., NY* **211** 249
- [60] Eckardt A and Holthaus M 2008 Dressed matter waves *J. Phys. Conf. Ser.* **99** 012007

- [61] von Neumann J and Wigner E 1929 Über das Verhalten von Eigenwerten bei Adiabatischen Prozessen *Phys. Z.* **30** 467 Reprinted in 1961 *John von Neumann—Collected Works* Taub A H vol 1 (New York: Pergamon) p 553
- [62] Hogg T and Huberman B A 1982 Recurrence phenomena in quantum dynamics *Phys. Rev. Lett.* **48** 711
- [63] Bunimovich L, Jauslin H R, Lebowitz J L, Pellegrinotti A and Nielaba P 1991 Diffusive energy growth in classical and quantum driven oscillators *J. Stat. Phys.* **62** 793
- [64] Combescure M 1988 The quantum stability problem for some class of time-dependent Hamiltonians *Ann. Phys., NY* **185** 86
- [65] Casati G, Chirikov B V, Izrailev F M and Ford J 1979 Stochastic behavior of a quantum pendulum under a periodic perturbation *Stochastic Behavior in Classical and Quantum Hamiltonian Systems (Lecture Notes in Physics* vol 93) (New York: Springer) p 334
- [66] Casati G and Gurarie I 1984 Non-recurrent behaviour in quantum dynamics *Commun. Math. Phys.* **95** 121
- [67] Eckardt A and Anisimovas E 2015 High-frequency approximation for periodically driven quantum systems from a Floquet-space perspective *New J. Phys.* **17** 093039
- [68] Yajima K 1982 Resonances for the AC-Stark effect *Commun. Math. Phys.* **87** 331
- [69] Holthaus M 1992 The quantum theory of an ideal superlattice responding to far-infrared laser radiation *Z. Phys. B* **89** 251
- [70] Drese K and Holthaus M 1997 Ultracold atoms in modulated standing light waves *Chem. Phys.* **217** 201 (Special issue: *Dynamics of Driven Quantum Systems*)
- [71] Arlinghaus S and Holthaus M 2011 Generalized acceleration theorem for spatiotemporal Bloch waves *Phys. Rev. B* **84** 054301
- [72] Wannier G H 1960 Wave functions and effective Hamiltonian for Bloch electrons in an electric field *Phys. Rev.* **117** 432
- [73] Avron J E, Zak J, Grossmann A and Gunther L 1977 Instability of the continuous spectrum: the N-band Stark ladder *J. Math. Phys.* **18** 918
- [74] Holthaus M and Hone D W 1996 Localization effects in ac-driven tight binding lattices *Phil. Mag. B* **74** 105
- [75] Drese K and Holthaus M 1996 Anderson localization in an ac-driven two-band model *J. Phys.: Condens. Matter* **8** 1193
- [76] See, e.g., Gavrila M (ed) 1992 *Atoms in Intense Laser Fields (Advances in Atomic, Molecular, and Optical Physics, Supplement 1)* (San Diego, CA: Academic Press)
- [77] Kohn W 1959 Analytic properties of Bloch waves and Wannier functions *Phys. Rev.* **115** 809
- [78] Boers D J, Goedeke B, Hinrichs D and Holthaus M 2007 Mobility edges in bichromatic optical lattices *Phys. Rev. A* **75** 063404
- [79] Holthaus M 1992 Collapse of minibands in far-infrared irradiated superlattices *Phys. Rev. Lett.* **69** 351
- [80] Olver F W J 1970 Bessel functions of integer order *Handbook of Mathematical Functions* ed M Abramowitz and I A Stegun (New York: Dover) ch 9
- [81] Arlinghaus S and Holthaus M 2010 Driven optical lattices as strong-field simulators *Phys. Rev. A* **81** 063612
- [82] Arlinghaus S and Holthaus M 2012 ac Stark shift and multiphotonlike resonances in low-frequency-driven optical lattices *Phys. Rev. A* **85** 063601
- [83] Arimondo E, Ciampini D, Eckardt A, Holthaus M and Morsch O 2012 Kilohertz-driven Bose–Einstein condensates in optical lattices *Adv. At. Mol. Opt. Phys.* **61** 515
- [84] Madison K W, Fischer M C, Diener R B, Niu Q and Raizen M G 1998 Dynamical Bloch band suppression in an optical lattice *Phys. Rev. Lett.* **81** 5093
- [85] Dunlap D H and Kenkre V M 1986 Dynamic localization of a charged particle moving under the influence of an electric field *Phys. Rev. B* **34** 3625
- [86] Arlinghaus S, Langemeyer M and Holthaus M 2011 Dynamic localization in optical lattices *Dynamical Tunneling—Theory and Experiment* ed S Keshavamurthy and P Schlagheck (London/ Boca Raton, FL: Taylor and Francis/ CRC Press) p 289
- [87] Aubry S and André G 1980 Analyticity breaking and Anderson localization in incommensurate lattices *Ann. Israel Phys. Soc.* **3** 133
- [88] Sokoloff J B 1985 Unusual band structure, wave functions and electrical conductance in crystals with incommensurate periodic potentials *Phys. Rep.* **126** 189
- [89] Drese K and Holthaus M 1997 Exploring a metal-insulator transition with ultracold atoms in standing light waves? *Phys. Rev. Lett.* **78** 2932
- [90] Holthaus M, Ristow G H and Hone D W 1995 ac-field-controlled Anderson localization in disordered semiconductor superlattices *Phys. Rev. Lett.* **75** 3914
- [91] Eckardt A, Weiss C and Holthaus M 2005 Superfluid-insulator transition in a periodically driven optical lattice *Phys. Rev. Lett.* **95** 260404
- [92] Eckardt A and Holthaus M 2007 AC-induced superfluidity *Europhys. Lett.* **80** 50004
- [93] Greiner M, Mandel O, Esslinger T, Hänsch T W and Bloch I 2002 Quantum phase transition from a superfluid to a Mott insulator in a gas of ultracold atoms *Nature* **415** 39
- [94] Creffield C E and Monteiro T S 2006 Tuning the Mott transition in a Bose–Einstein condensate by multiple photon absorption *Phys. Rev. Lett.* **96** 210403
- [95] Weinberg M, Ölschläger C, Sträter C, Prell S, Eckardt A, Sengstock K and Simonet J 2015 Multiphoton excitations of quantum gases in driven optical lattices *Phys. Rev. A* **92** 043621
- [96] Arlinghaus S and Holthaus M 2011 Controlled wave packet manipulation with driven optical lattices *Phys. Rev. A* **84** 063617
- [97] Judson R S and Rabitz H 1992 Teaching lasers to control molecules *Phys. Rev. Lett.* **68** 1500
- [98] Rice S A and Zhao M 2000 *Optical Control of Molecular Dynamics* (New York: Wiley)
- [99] Shapiro M and Brumer P 2003 Coherent control of molecular dynamics *Rep. Prog. Phys.* **66** 859